Prepared for Submission, Oct xx, 2019

SLAU2 applied to Two-Dimensional, Ideal Magnetohydrodynamics Simulations

Keiichi Kitamura [a, *] , Tomohiro Mamashita [a], and Dongsu Ryu [b]

a) Yokohama National University, 79-5 Tokiwadai, Hodogaya-ku, Yokohama, Kanagawa 240-8501, Japan

b) Ulsan National Institute of Science and Technology, UNIST-gil 50, Ulsan, 44919, Republic of Korea

Abstract

SLAU2 (Simple Low-dissipation Advection-Upstream-splitting-method 2) numerical flux function, one of AUSM-type methods (3-wave solver), originally developed and widely used in gasdynamics, has been applied to two-dimensional magnetohydrodynamics (MHD) simulations. According to numerical tests for a wide range of flow and magnetic conditions, its reliability, efficiency, and accuracy have been demonstrated: i) Robustness of SLAU2 against shock-anomalies (e.g., carbuncle phenomena) has been confirmed in the MHD-extended version of our hypersonic flow test; ii) The computational cost has been reduced for approximately 3% compared with HLLD (Harten-Lax-van_Leer with Discontinuities), a more expensive, 5-wave solver; iii) Nevertheless, its solution qualities are almost equal to those of HLLD, as opposed to very diffused HLL solutions. For benchmark tests, detailed and important flow physics such as multidimensional shock/shock interactions have been successfully reproduced by SLAU2. We hope that SLAU2 will contribute to further progress of the astrophysics and other research fields.

[*] corresponding author; tel: +81-45-339-3876, e-mail address: kitamura@ynu.ac.jp

Keywords: SLAU2, MHD, Euler Fluxes

1. Introduction

There are continued attentions to accurate, robust, yet economical magnetohydrodynamics (MHD) simulations such as in astrophysics [1, 2, 3], aerospace engineering [4], and nuclear engineering communities [5, 6]. In order to accomplish such simulations, it is of great importance to establish and/or employ a reliable numerical method in each part of the computational process, such as reconstruction methods [7, 8], slope limiters [9], numerical flux functions [10, 11, 12, 13], time integration methods [14], and divergence treatments [15-19]. In this work, a particular attention will be paid to the flux functions (that calculate fluxes through cell interfaces based on the interpolated variables there), since they affect both the accuracy and the qualitative behavior of the numerical solutions, in the worst case yielding what appear to be incorrect weak solutions, often referred to as "anomalous solutions" [20-26]. Let us provisionally categorize the flux functions into four groups according to the numbers of resolved waves and their responses to the shocks, as shown in Fig. 1.

- Group I: Full-wave solvers (or 7-wave solvers) – Roe [27-31] (extended from gasdynamics [9]) and HLLI (Harten-Lax-van_Leer with Intermediate waves) [32]. They capture all the seven waves in MHD, i.e., left/right-running fast waves, Alfvén waves, slow waves, and an entropy wave. They are accurate in resolving detailed flow physics. However, they tend to produce anomalous solutions at the captured shocks (e.g., "*carbuncle*" phenomena [21-26]), as pointed out by Liou [33] and confirmed by many researchers in gasdynamics [21] and MHD [3]. In addition, especially in MHD, treating all the seven waves is computationally expensive.
- Group II: 5-wave solver – HLLD (Harten-Lax-van_Leer with Discontinuities) [11], which is an extended version of HLLC (Harten-Lax-van_Leer with Contact) from gasdynamics. This Riemann solver omits slow waves, and hence, captures left/right fast waves, left/right Alfvén waves, and the entropy wave. While this solver does not recognize the slow waves, it produces satisfactory solutions as demonstrated by many subsequent works [34, 35, 36].
- Group III: 3-wave solvers – AUSM (Advection-Upstream-Splitting-Method)-type solvers [37, 38, 39], E-CUSP (Energy-conservative Convective Upwind and Split Pressure) [40], and HLLC [41, 42]. These recent AUSM solvers inherit the spirit of the earlier AUSM, i.e., they possess both the simplicity of flux-

vector-splitting (FVS) (e.g. Van Leer's [43]) and the contact-resolving nature of the flux-difference-splitting (FDS) (e.g., Roe). In MHD, they treat the fast waves (the sound waves in gasdynamics) in both directions along with the entropy wave. In addition to this *simplification*, they eliminate the need of the complicated eigensystems in MHD for *efficiency*. SLAU2 [12] was extended to "1D" MHD in [37]. AUSMPW+ (AUSM by Pressure-based Weight functions +) [44] was applied to MHD by Han et al. [39], but with only a limited multidimensional case, which was later further extended to several 2D simulations by Xisto et al. [38] and enhanced in [37]. They are known to be *very robust* against the shock anomalies in gasdynamics [12, 25, 45]. Moreover, they can capture the contact discontinuity *accurately*, and hence, boundary-layers in viscous simulations too [12, 44]. E-CUSP [46] has a similar structure of the AUSM-type fluxes and was extended to MHD in [40], although it will be more diffusive according to its formulation. HLLC, on the other hand, is known to be as vulnerable as Roe solver to the carbuncle [21, 47], probably because it can be written in a very similar manner to the Roe solver in the eigenmatrix-free expression [48, 49]. Li [41] and Gurski [42] tried to extend HLLC [50] to MHD, but their versions of HLLC are of course not capable of resolving Alfvén waves.

- Group IV: 2-wave solvers – (2-wave) HLL [13] (a "3-wave" HLL was also proposed there, which might be categorized into Group III, as well as Linde's version [73]), Rusanov (or also known as Local Lax Friedrich) [51], and typical FVS methods. An MHD-extended HLL was proposed in [52]. These solvers omit the entropy wave, and resolve only the left and right fastest waves (i.e., fast waves in MHD, and sound waves in gasdynamics). As a natural consequence, a contact discontinuity and a boundary-layer are smeared. However, as opposed to Roe flux for instance, they are very robust in capturing shocks, again as explained in [33]. In ATHENA [35] code, HLL is hybridized with Roe or HLLD such that HLL is used only at the shocks in a multidimentional manner [24, 53], although universality of such techniques is not fully guaranteed [25, 54]. What is more, such a hybridization adds extra cost and complexity to the numerical code.

As reviewed above, AUSM-type solvers in Group III appear to be promising because they feature *robustness, accuracy, efficiency, and simplicity* by itself. Specifically, SLAU2 is nowadays utilized by many practitioners and incorporated in many numerical codes, such as FaSTAR [55], LS-FLOW [56], and SU2 (Stanford University Unstructured code) [57]. It features robustness against the shock anomalies [12], and also capability of all-speed

(including an incompressible regime, such as the solar convective zone [58, 59, 60, 61] or International Thermonuclear Experimental Reactor (ITER) [5, 6]) flow computations [20]. Furthermore, in contrast with AUSM$^+$-up [62], no user-specified parameters are required such as "cutoff Mach number" [32, 36], that significantly affect the solutions and sometimes need experts' care.

Kitamura & Balsara [37] proposed SLAU2 (Group III) in 1D MHD and extensively tested its performance (such as in 1D MHD shocktube tests [27, 28]). Overall, SLAU2 produced good solutions, except for very severe cases in which slight oscillations were observed [37]. However, the performance of SLAU2 in more realistic, multidimensional problems was not surveyed in [37]. In fact, *many flow physics such as a vortex, an oblique shock, a boundary-layer, shock- or contact-induced instabilities (e.g., carbuncle), and their interactions are multidimensional*. In addition, however good the 1D solution is, it does not guarantee multidimensional accuracy or robustness of the computation as evident in gasdynamics simulations [24, 25].

In this work, therefore, the SLAU2 in MHD will be thoroughly investigated in an MHD-extended carbuncle test and well-known benchmark cases in 2D, as a natural extension of the previous work. Through these numerical tests, as a first goal of the present work, both strengths (in most cases, e.g., robustness against shock-anomalies) and limitations (in a limited case) of SLAU2 in 2D MHD are expected to be discovered and highlighted. It is also expected that these findings will contribute to further developments of numerical algorithms in the future, as a second goal. In multidimensions, it is reported that the treatment of divergence of magnetic field is necessary, whereas its compatibility with SLAU2 is still questionable. Among many methods for divergence-free treatments on magnetic field ($\nabla \cdot \mathbf{B} = 0$) [15-19], we select a hyperbolic divergence-cleaning method [15] which is already incorporated in CANS+ [34], an open MHD code developed in Japan. In order for SLAU2 in MHD to be readily available to many potential users/practitioners (a third goal), we employed CANS+ code rather than in-house one (in [37]) throughout the paper.

This paper is organized as follows. Section 2 will describe the governing equations. In Sec. 3, its discretization, and the numerical methods to solve these equations will be presented, in particular SLAU2 in MHD. Then, two-dimensional MHD numerical tests will be conducted to survey the performance of SLAU2 in Sec. 4. Finally, Sec. 5 will summarize the present work.

2. Governing Equations

The governing equations are the compressible MHD equations as follows:

$$\frac{\partial \mathbf{Q}}{\partial t}+\frac{\partial \mathbf{F}}{\partial x}+\frac{\partial \mathbf{G}}{\partial y}+\frac{\partial \mathbf{H}}{\partial z}=0 \tag{1a}$$

$$\mathbf{Q}=\begin{bmatrix}\rho\\ \rho u\\ \rho v\\ \rho w\\ \rho E\\ B_x\\ B_y\\ B_z\end{bmatrix},\mathbf{F}=\begin{bmatrix}\rho u\\ \rho u^2+p_G-B_x^2\\ \rho uv-B_xB_y\\ \rho uw-B_xB_z\\ \rho uH-B_x(\mathbf{u}\cdot\mathbf{B})\\ 0\\ uB_y-vB_x\\ uB_z-wB_x\end{bmatrix},\mathbf{G}=\begin{bmatrix}\rho v\\ \rho vu-B_yB_x\\ \rho v^2+p_G-B_y^2\\ \rho vw-B_yB_z\\ \rho vH-B_y(\mathbf{u}\cdot\mathbf{B})\\ vB_x-uB_y\\ 0\\ vB_z-wB_y\end{bmatrix},\mathbf{H}=\begin{bmatrix}\rho w\\ \rho wu-B_zB_x\\ \rho wv-B_zB_y\\ \rho w^2+p_G-B_z^2\\ \rho wH-B_z(\mathbf{u}\cdot\mathbf{B})\\ wB_x-uB_z\\ wB_y-vB_z\\ 0\end{bmatrix} \tag{1b}$$

where $\mathbf{Q}$ is the vector of conservative variables, ρ is the density, $\mathbf{u} = (u, v, w)^T$ is velocity, p gas pressure, p_G global pressure ($p_G = p + B^2/2$), $\mathbf{B}$ magnetic field [$B^2 = \mathbf{B}\cdot\mathbf{B}$; $\mathbf{B} = (B_x, B_y, B_z)^T$], E total energy per unit mass [$E = (p/\rho)/(\gamma-1)+0.5(u^2+v^2+w^2)+0.5B^2/\rho$], and H total enthalpy [$H = E + (p/\rho)$]. The working gas is assumed as the calorically perfect gas with the specific heat ratio γ. The first five equations are Euler equations, whereas the 6th – 8th equations comprise Faraday's law for MHD, which is a part of the Maxwell equations. In addition, a scalar potential ψ is solved in a similar manner as a hyperbolic divergence cleaning method [15].

Then, Eq. (1a) is solved with a finite-volume code, and can be written in the delta form as:

$$\Delta\mathbf{Q}_i=-\frac{\Delta t}{\Delta V}\left(\mathbf{F}_{i-1/2}-\mathbf{F}_{i+1/2}\right) \tag{2}$$

where $\Delta\mathbf{Q}_i$ is change of conservative variables in time, Δt is the time step, ΔV stands for the volume of the cell, and $\mathbf{F}_{i\pm1/2}$ is the inviscid (Euler) flux through the cell-interface (which separates the cell i and its neighbor cell $i\pm1$), respectively. Details of the inviscid fluxes are explained below.

3. Numerical Methods

3.1 Flux Function

SLAU2 was first extended to 1D MHD in [37]. As discussed in [37], the Euler equations (the gas flow part, 1st-5th equations of Eq.(1)) and Maxwell equations (the magnetic field, 6th – 8th) are handled separately. Let us begin from the Euler equations part, i.e., the first five components of Eq.(1).

$$\mathbf{F}_{SLAU2(Euler)} = \frac{\dot{m}+|\dot{m}|}{2}\boldsymbol{\Psi}^{+}_{Euler} + \frac{\dot{m}-|\dot{m}|}{2}\boldsymbol{\Psi}^{-}_{Euler} + \mathbf{P}_{Euler} + B_{1/2}\frac{\boldsymbol{\Psi}^{+}_{Euler,B}+\boldsymbol{\Psi}^{-}_{Euler,B}}{2} \tag{3a}$$

$$\boldsymbol{\Psi}^{+}_{Euler} = \left(1, u_L, v_L, w_L, H_L\right)^T; \quad \boldsymbol{\Psi}^{-}_{Euler} = \left(1, u_R, v_R, w_R, H_R\right)^T,$$
$$\boldsymbol{\Psi}^{+}_{Euler,B} = \left(0, -B_{xL}, -B_{yL}, -B_{zL}, 0\right)^T; \quad \boldsymbol{\Psi}^{+}_{Euler,B} = \left(0, -B_{xR}, -B_{yR}, -B_{zR}, 0\right)^T \tag{3b}$$

$$\mathbf{P}_{Euler} = \begin{pmatrix} 0 \\ \widetilde{p} \\ 0 \\ 0 \\ \mathrm{P}^{+}\cdot\left\{-\left(u_L B_{L,x} + v_L B_{L,y} + w_L B_{L,z}\right)B_{1/2}\right\} + \mathrm{P}^{-}\cdot\left\{-\left(u_R B_{R,x} + v_R B_{R,y} + w_R B_{R,z}\right)B_{1/2}\right\} \end{pmatrix} \tag{3c}$$

$$\mathrm{P}^{+} = \begin{cases} \frac{1}{2}\left(1+sign\left(M_L\right)\right), & if\ |M_L| \ge 1 \\ \frac{1}{4}\left(M_L+1\right)^2\left(2-M_L\right), & otherwise \end{cases} \tag{3d}$$

$$\mathrm{P}^{-} = \begin{cases} \frac{1}{2}\left(1-sign\left(M_R\right)\right), & if\ |M_R| \ge 1 \\ \frac{1}{4}\left(M_R-1\right)^2\left(2+M_R\right), & otherwise \end{cases} \tag{3e}$$

where $B_{1/2} = \dfrac{B_{x,L}+B_{x,R}}{2}$ as in [39]. The mass flux is

$$\left(\dot{m}\right)_{SLAU2} = \frac{1}{2}\left\{\rho_L\left(u_L + \left|\overline{V}_n\right|^{+}\right) + \rho_R\left(u_R - \left|\overline{V}_n\right|^{-}\right) - \frac{\chi}{\overline{c}}\left(p_{G,R}-p_{G,L}\right)\right\} \tag{4a}$$

$$|\overline{V}_n|^{+} = (1-g)\,|\overline{V}_n| + g\,|u_L|, \quad |\overline{V}_n|^{-} = (1-g)\,|\overline{V}_n| + g\,|u_R| \tag{4b}$$

$$\left|\overline{V}_n\right| = \frac{\rho_L|u_L| + \rho_R|u_R|}{\rho_L+\rho_R} \tag{4c}$$

$$g = -\max\left[\min\left(M_L, 0\right), -1\right]\cdot\min\left[\max\left(M_R, 0\right), 1\right] \quad \in [0,1] \tag{4d}$$

where p_G is the global pressure ($p_G = p + B^2/2$), and

$$\chi = (1-\widehat{M})^2 \tag{4e}$$

$$\widehat{M} = \min\left(1.0, \frac{1}{\overline{c}}\sqrt{\frac{\mathbf{u}_L^{\,2}+\mathbf{u}_R^{\,2}}{2}}\right) \tag{4f}$$

$$M_L = \frac{u_L}{\overline{c}}, M_R = \frac{u_R}{\overline{c}} \tag{4g}$$

$$\overline{c} = \frac{c_{f,L}+c_{f,R}}{2} \tag{4h}$$

where c is, in this MHD case, the fast magnetosonic speed,

$$c_{f,L/R}^2 = \frac{1}{2}\left\{ a_{L/R}^2 + \frac{\mathbf{B}_{L/R}^2}{\rho_{L/R}} + \sqrt{\left(a_{L/R}^2 + \frac{\mathbf{B}_{L/R}^2}{\rho_{L/R}} \right)^2 - 4a_{L/R}^2 \frac{B_{x,L/R}^2}{\rho_{L/R}}} \right\} \tag{4i}$$

and $a_{L/R}$ is the gas speed of sound, $a_{L/R}^2 = \dfrac{\gamma p_{L/R}}{\rho_{L/R}}$.

Then, the pressure flux is:

$$\left(\widetilde{p}\right)_{SLAU2} = \frac{p_{G,L} + p_{G,R}}{2} + \frac{\mathrm{P}^+ - \mathrm{P}^-}{2}\left(p_{G,L} - p_{G,R}\right) + \sqrt{\frac{\mathbf{u}_L{}^2 + \mathbf{u}_R{}^2}{2}} \cdot \left(\mathrm{P}^+ + \mathrm{P}^- - 1\right)\overline{\rho c} \tag{4j}$$

$$\overline{\rho} = \frac{\rho_L + \rho_R}{2} \tag{4k}$$

for the gasdynamics part (1st – 5th lines of Eq.(1)). On the other hand, the magnetic part, i.e., 6th – 8th lines are solved by simple HLL manner:

$$\mathbf{F}_{SLAU2(Maxwell)} = \mathbf{F}_{HLL(Maxwell)} = \frac{S_R\mathbf{F}_L - S_L\mathbf{F}_R + S_L S_R\left(\mathbf{Q}_R - \mathbf{Q}_L\right)}{S_R - S_L} \tag{5a}$$

$$S_R = \max\left(u_L, \quad u_R\right) + \max\left(c_{f,L}, \quad c_{f,R}\right), \quad S_L = \min\left(u_L, \quad u_R\right) - \max\left(c_{f,L}, \quad c_{f,R}\right) \tag{5b}$$

where $S_{L/R}$ are "signal" speeds traveling in lift and right directions, respectively. With this simplification of the Faraday's law treatment, the robustness of SLAU2 was dramatically improved in 1D. The key idea behind this modification in [37] was that we eliminated the dissipation term from the magnetic part, which would have contaminated the magnetic field. It should be noted that there was another variant proposed in [37] which adopted the early AUSM manner instead of HLL for the magnetic part, resulted in very similar solutions and performances (thus, omitted in this paper). In addition, Eq.(5b) uses only local velocities and the fast speeds for simplicity, whereas in [37] the Roe average values were used. The results in Sec. 4 will confirm the validity of this change.

Furthermore, in order to take Alfvén waves into account and enhance the stability at strong shocks, we introduced the following Alfvén speed,

$$S_{A,R} = \max\left(u_R + c_{A,R}, \quad 0\right), \quad S_{A,L} = \min\left(u_L - c_{A,L}, \quad 0\right) \tag{6}$$

and a strong-shock-detector using the pressure function borrowed from AUSMPW+ flux function (but with c_A-weight included) [39, 44],

$$w = \min\left(\frac{p_{G,L}}{p_{G,R}}, \quad \frac{p_{G,R}}{p_{G,L}}, \quad \frac{c_{A,L}^2}{c_{A,R}^2}, \quad \frac{c_{A,R}^2}{c_{A,L}^2} \right)^3 \tag{7a}$$

where

$$c_{A,L/R}^2 = \frac{\mathbf{B}_{L/R}^2}{\rho_{L/R}} \tag{7b}$$

Then, the following new signal speeds are employed that considered both the fast speed and Alfvén speeds,

$$S_{R,new} = \max\big((1-w)S_R + wS_{A,R},\quad 0\big),\quad S_{L,new} = \min\big((1-w)S_L + wS_{A,L},\quad 0\big) \tag{8}$$

which will be substituted for Eq.(5a). The point here is that, when there are no strong shocks in the solution ($w \approx 1$), the flux (for the magnetic field *only*) is soon switched from fast-speed-based HLL [Eq.(5b)] to the Alfvén-speed-based HLL [Eq.(6)], while SLAU2 for the Euler equation part is unaltered. This version will be simply called "SLAU2" in this paper, and will be tested in Section 4.

3.2 Other Aspects

The spatial accuracy is two by MUSCL [7] with the minmod limiter [9], or five by MP5 (5th-order Monotonicity-Preserving scheme) (only in 4.7) [8], according to the selected reconstruction method. The temporal order of accuracy is three by an explicit TVD-RK (Total-Variation-Diminishing Runge-Kutta) method [14]. The divergence-free treatment for the magnetic field is realized by the hyperbolic divergence cleaning [15]. These detailed descriptions can be found in the original CANS+ paper [34].

4. 2D MHD Numerical Tests

A series of 2D test problems are conducted. The solutions of HLL or HLLD are also presented in selected cases for comparisons. We did not include HLLC solver because i) it is also a 3-wave solver, and ii) in spite of i), it showed carbuncle solutions as frequently as Roe, as demonstrated in [45].

4.1 2D-Extended Ryu-Jones Shocktubet

The Ryu-Jones shocktube test [28] has been extensively conducted to investigate the method's capability in 1D MHD, and SLAU2 actually showed the satisfactory solution in [37]. Ryu et al. extended this test to two dimensions in [63] in which waves travel in diagonal directions in the computational domain, with no detailed explanations on the computational setup. Here we prepared the same initial conditions, but with simpler boundary conditions on a

rectangular space [0, 1] x [0, 0.25] divided by 400 x 100 squares (Fig. 2).

- $(\rho, u, v, w, p, B_x, B_y, B_z)_L = (1.08, 1.19/\sqrt{2}, 1.21/\sqrt{2}, 0.5, 0.95, -1.6/\sqrt{8\pi}, 5.6/\sqrt{8\pi}, 2/\sqrt{8\pi})$ for $x + y < 0.625$
- $(\rho, u, v, w, p, B_x, B_y, B_z)_R = (1, 0, 0, 0, 1, -2/\sqrt{8\pi}, 6/\sqrt{8\pi}, 2/\sqrt{8\pi})$ for $x + y > 0.625$

with $\gamma = 5/3$. In order to treat the diagonal propagations of waves economically, we adopted a "shifted" periodical boundary condition, in which, for example, the cells of $(i, j) = (101, 0)$ and $(1, 100)$ are continuously connected. The simple outlet condition is applied to the other cells. The simulations are run until $t = 0.04 \times 2^{0.5}$ with TVD-RK3 (CFL = 0.6) for time integration and MP5 for spatial reconstruction [8].

The density, pressure, and magnetic field profiles along x-$y = 0.75$ line are plotted in Fig. 3 and Fig. 4. These figures demonstrate that the present computations were successful, including the shifted boundary setup. The solution of SLAU2 (for all the density, pressure, magnetic field in the wave-perpendicular component in the computational plane $B_{perp} = (-B_x + B_y)/2^{0.5}$, and the component out of the plane B_z) is very similar to the 5-wave HLLD solution, and reproduces the reference solution (created by HLL on a 4,000 x 1,000 grid) and the well-known 1D Ryu-Jones solutions [28].

4.2 MHD Carbuncle Test

This test was initially proposed for gasdynamics by Kitamura, Roe, and Ismail in [25], and the MHD version of the similar test was conducted in [3]. Here, the "1-1/2-D test" in [25] is directly extended to MHD (Fig. 5). We prepared a rectangular computational domain [0, 1] x [0, 0.5] filled with 50 x 25 squares, without any grid perturbations. Then, as the initial condition, the pre-shock condition is given at cells of $i \leq 12$, while the post-shock state according to the Rankine-Hugoniot condition is prescribed for $i \geq 14$; as for all the primitive variables $\boldsymbol{q}_M$ in the numerically-expressed shock internal zone, i.e., i=13th cell, values upstream ($\boldsymbol{q}_L$) and downstream ($\boldsymbol{q}_R$) the shock are blended according to the specified, initial shock location parameter $\varepsilon = 0.0, 0.1, \ldots 0.9$:

$$\mathbf{q}_M = \varepsilon \mathbf{q}_L + (1-\varepsilon)\mathbf{q}_R \tag{9}$$

This setup is justified by the fact that, according to [64], a mathematical expression inside the numerical shock inevitably exhibits at most 40% errors between the mass conservation law and the Hugoniot curve at Mach 10. It is also supported by many practical simulations in which the shock does not necessarily sit exactly on the grid lines but

resides on a few cells – in either case, the numerically captured shock may or may not be destabilized according to the chosen numerical methods, computational cells, flow conditions, etc. [21, 25, 45].

The left and right initial conditions for Mach 6, $\gamma = 5/3$ for instance, are as follows:

- $(\rho, u, v, w, p, B_x, B_y, B_z)_L = (1, 6, 0, 0, 1/\gamma, 25, 0, 0)$ for $i < 12$
- $(\rho, u, v, w, p, B_x, B_y, B_z)_R = (3.692, 1.625, 0, 0, 26.85, 25, 0, 0)$ for $i > 14$

and if $M = 20$,

- $(\rho, u, v, w, p, B_x, B_y, B_z)_L = (1, 20, 0, 0, 1/\gamma, 25, 0, 0)$ for $i < 12$
- $(\rho, u, v, w, p, B_x, B_y, B_z)_R = (3.970, 5.0375, 0, 0, 299.85, 25, 0, 0)$ for $i > 14$

The inlet condition (Mach 6 or 20) is prescribed at the left boundary; the outlet condition with the fixed post-shock pressure is imposed at the right boundary; specified at the top and the bottom boundaries are the periodic condition. The computations are carried out with spatially first-order (which best highlights the difference arising from shock anomalies [25]) or second-order (by MUSCL, denoted as "MUSCL2"), third-order TVD-RK time integration (hereafter, "TVD-RK3") for 40,000 timesteps (CFL=0.5).

Typical solutions (Mach 20, ε=0.0 or 0.5, first-order in space) are presented in Fig. 6, with no signs of carbuncle or other shock anomalies observed (nearly the same solutions were obtained for the other initial parameters). Therefore, *robustness against shock anomalous solutions such as carbuncle has been confirmed for SLAU2 in MHD* (with a broader shock as designed than HLLD, which apparently reached different shock locations according to the initial condition), as well as in gasdynamics [12].

4.3 Orzag-Tang Vortex

This is a typical 2D MHD problem [65] conducted in many computational MHD papers [18, 35, 38, 39, 40]. The following initial condition triggers a complicated MHD flowfield involving several shock interactions:

- $(\rho, u, v, w, p, B_x, B_y, B_z) = (\gamma^2, -\sin(y), \sin(x), 0, \gamma, -\sin(y), \sin(2x), 0)$

with $\gamma = 5/3$. The uniform 100 x 100 cells cover $[0, 2\pi]$ x $[2\pi]$. This computational grid is relatively coarse, which will better highlight differences among solutions by different numerical fluxes. The periodic condition is applied to all the four boundaries. The computations are conducted until $t = \pi$ with MUSCL2 and TVD-RK3 (CFL = 0.3).

In Fig. 7, density and pressure contours are displayed for SLAU2, HLLD, and HLL. They overall look similar and resemble the reported solutions in literature [18, 35, 38, 39, 40], capturing important physics such as shock

interactions. However, HLL appears to be more diffusive than the others. In order to take a closer look, we plotted the density and pressure profiles along y = 1 line in Fig. 8. It is seen that SLAU2 (3-wave-solver) and HLLD (5-wave-solver) produced almost the same results but the HLL (2-wave-solver) solution was rather diffused especially around x = 1.4 in the density, whereas in the pressure these three methods yielded almost the same solutions (SLAU2 solution is slightly closer to HLL than HLLD in pressure, though – this trend is also evident in the center zone of pressure in each right figure of Fig.8). From this example, it has been demonstrated that *SLAU2 successfully handled this 2D MHD problem involving complex shock interactions as well as HLLD*. Nevertheless, the computational cost of the SLAU2 case is 3% (which is slight but indeed) lower than the HLLD case for this particular problem (but common to almost all the other test problems), as summarized in Table 1. It is worth pointing out that this difference will rise in three-dimensional problems.

4.4 MHD Blast Wave

This problem was conducted by [17, 38, 66, 67]. There are several variants for this problem, but we chose the following setup as the initial condition:

- $(\rho, u, v, w, p, B_x, B_y, B_z) = (1, 0, 0, 0, 100, 10/\sqrt{2}, 10/\sqrt{2}, 0)$ inside a circle centered at $(x, y) = (0.5, 0.5)$ with 0.125 radius
- $(\rho, u, v, w, p, B_x, B_y, B_z) = (1, 0, 0, 0, 1, 10/\sqrt{2}, 10/\sqrt{2}, 0)$ elsewhere ($\beta = 2p/|\mathbf{B}|^2 = 0.001$)

with γ = 1.4. The 100 x 100 computational cells are uniformly distributed in a [0, 1] x [0, 1] domain, having the periodic boundary conditions on all the four edges, as in the previous example. The computational methods (MUSCL2 and TVD-RK3, CFL = 0.3) are also the same as in the previous test. The computations were successful without suffering from negative pressure [38] or serious oscillations, and the solutions are compared at t = 0.02 in Fig. 9. All the solutions preserve symmetry with respect to the magnetic field and nearly reproduce the published solution [66], with slight differences (HLL is smooth yet diffused, especially in the direction orthogonal to the magnetic field). These observations are confirmed from Fig. 10 where diagonal distributions of density and pressure are compared.

The above ambient condition corresponds to a small value of the plasma beta $\beta = 2p/|\mathbf{B}|^2 = 0.001$. Xisto et al. [38] failed the computation under this setup, and claimed that it attributed to this small β. Thus, they alternatively

employed the following larger β:

- (ρ, *u, v, w, p,* B_x, B_y, B_z) = (1, 0, 0, 0, 1000, $25/\sqrt{8\pi}$, $25/\sqrt{8\pi}$, 0) inside a circle centered at (x, y) = (0.5, 0.5) with 0.1 radius
- (ρ, *u, v, w, p,* B_x, B_y, B_z) = (1, 0, 0, 0, 0.1, $25/\sqrt{8\pi}$, $25/\sqrt{8\pi}$, 0) elsewhere (β = 0.004)

again, with γ = 1.4. Figure 11 displays the solutions at t = 0.012 obtained by SLAU2, HLLD, and HLL for this second setup. These solutions are again satisfactory, and very similar to each other and those reported in [38].

4.5 MHD Rotor

This problem was conducted in [17, 18, 35, 38, 40]. We followed Xisto et al.'s setup [38]:

- (ρ, *u, v, w, p,* B_x, B_y, B_z) = (10, -2y/0.1, 2x/0.1, 0, 1, $5/\sqrt{4\pi}$, 0, 0) for r < 0.1 (inside the cylinder)
- (ρ, *u, v, w, p,* B_x, B_y, B_z) = (1+9f(r), -2f(r)y/r, 2f(r)x/r, 0, 1, $5/\sqrt{4\pi}$, 0, 0) for 0.1 < r < 0.115 (buffer)
- (ρ, *u, v, w, p,* B_x, B_y, B_z) = (1, 0, 0, 0, 1, $5/\sqrt{4\pi}$, 0, 0) for 0.115 < r (ambient)

with γ = 1.4 as the initial condition. The r is given as $r = [(x - 0.5)^2 + (y - 0.5)^2]^{0.5}$ from the cylinder center (x, y) = (0.5, 0.5) with its radius 0.1. The function $f(r)$ is defined as $f(r) = (200/3)\ (0.115 - r)$, which linearly interpolates the buffer region from the cylinder to the ambient.

Computational grids of evenly spaced 100 x 100 cells and 50 x 50 cells are prepared for a [0, 1] x [0, 1] computational space, with the periodic conditions applied to all the boundaries. The computational methods (MUSCL2 and TVD-RK3 with CFL = 0.3) are again the same as in the above tests. The results at t = 0.15 are compared in Fig. 12 (100x100 cells) and Fig. 13 (50x50 cells).

These solutions look similar to each other on 100x100 cells, capturing all the important physics and match well with the others' solutions (Fig. 12). On 50x50 cells (Fig. 13), however, the HLLD solution is slightly more diffused than the SLAU2 solution, and the HLL solution is further smeared especially in the density plots. Thus, again, SLAU2 can produce nearly the same result as HLLD's even in this torsional-Alfvén-wave-featured MHD field. This is more clearly seen from Fig. 14 where density and pressure profiles along x=0.5 line are compared (especially in the density double peak near y=0.36 and 0.6). In addition, Shen et al. [40] were unable to compute this problem using E-CUSP, unless the spatial accuracy was lowered to one. Thus, these solutions *demonstrate the robustness of SLAU2 in 2D MHD*, again.

4.6 MHD Cloud/Shock Interaction

This problem deals with a cloud/shock interaction in MHD [18, 38, 68]. The left, right, and cloud initial conditions are as follows:

- $(\rho, u, v, w, p, B_x, B_y, B_z)_L$ = (3.86859, 0, 0, 0, 167.345, 0, 2.18262, 0) for x <0.6
- $(\rho, u, v, w, p, B_x, B_y, B_z)_R$ = (1, -11.2536, 0, 0, 1, 0, 0.564190, 0.564190) for x >0.6, r > 0.15
- $(\rho, u, v, w, p, B_x, B_y, B_z)_{cloud}$ = (10, -11.2536, 0, 0, 1, 0, 0.564190, 0.564190) for r < 0.15

with γ = 5/3. The r is given as $r = [(x - 0.8)^2 + (y - 0.5)^2]^{0.5}$ from the high-density cloud center (x, y) = (0.8, 0.5) with its radius 0.15. The [0, 1] x [0, 1] domain is filled with 200 x 200 squares. The supersonic inlet condition (i.e., all the variables are specified) is employed at the right boundary, whereas the outlet condition (i.e., all the variables are extrapolated from the interior neighbor cells) applies to the other boundaries. The computations are run with MUSCL2 and TVD-RK3 (CFL = 0.3), again. The solutions at t = 0.06 are displayed in Fig. 15.

The results involving shocks well reproduced the literature [18, 68]. The present SLAU2 and HLLD solutions resemble the mushroom-like cloud in [18, 68]; whereas the HLL is closer to the E-CUSP solution [38] which looks rather diffused with the rounded shape of the cloud on the same number of cells adopted. A careful reader may point out slightly larger oscillations near the shock in SLAU2 than those in HLLD. We feel they are acceptable, but a hybridization with a full-wave solver may suppress those oscillations, as done in our previous work for 1D MHD [37]. Figure 16 showing density profiles along x=0.3 also supports the above observation that SLAU2 and HLLD solutions are very similar, while HLL's is rather diffused.

4.7 Early Stage of Kelvin-Helmholtz Instability

This problem is solved on a very coarse grid, i.e., 16 x 20 cells splitting a [0, 5π] x [-10, 10] domain. The purpose of this test is to highlight the differences in solution resolutions on the initial stage of Kelvin-Helmholtz instability due to different numerical fluxes. In this problem, the following setup is employed as the initial conditions.

$$\rho = 1 + 0.05(2a - 1) \tag{10a}$$

$$u = -0.5\sqrt{1+\gamma}\,\tanh(y) \tag{10b}$$

$$v = 0.01\sqrt{1+\gamma}\,\sin(0.4x)/(\cosh(y))^2 \tag{10c}$$

$$w = 0 \tag{10d}$$

$$p = 1 - 0.5\left(B_x^2 + B_y^2 + B_z^2\right) = 0.5 \tag{10e}$$

$$B_x = 0 \tag{10f}$$

$$B_y = 0 \tag{10g}$$

$$B_z = 1 \tag{10h}$$

with $\gamma = 5/3$ and a is a random number created by the Fortran subroutine "random_number". The Eq.(10b) provides the velocity field with the shear profile [34], which will evolve and create a vortical flow structure as time progresses. The periodic conditions are applied to the left and right boundaries, while the outlet condition is used to the top and bottom. As for the computational methods, MP5 for spatial reconstruction [8] (the lower-order reconstruction failed to reproduce the flow structure on this very coarse grid), and TVD-RK3 (CFL = 0.3) for time integration are used. The solutions at t = 100 are compared in Fig. 17. As seen, even on this very coarse grid, SLAU2 and HLLD develop the expected vorticity field (indicted by high and low pressure spots) [69] as in [70], whereas HLL totally diffused such a structure. As a quantitative comparison, we plotted the time history of the root-mean-squares of the y-velocity [63], normalized by the values at t = 10, in Fig. 18. It is evident from this graph that SLAU2 and HLLD almost similarly developed the y-component velocity field (very similarly to the theoretical linear growth), whereas HLL diffused it.

In summary, SLAU2 produced reliable results in all the cases tested, without showing anomalies, severe oscillations, or losses of resolutions. The SLAU2 solutions demonstrated comparable qualities to the HLLD counterparts with better efficiency, and surpassed HLL which smeared out important physics such as density discontinuities and vorticities. We hope that SLAU2 will be incorporated into MHD codes (e.g., [35, 71, 72]), and will contribute to further progress of the astrophysics and the other related research areas.

5. Conclusions

The SLAU2 (Simple Low-dissipation Advection-Upstream-splitting-method 2) numerical flux function, one of AUSM-type methods (3-wave solver), originally developed and widely used in gasdynamics, has been applied to two-dimensional magnetohydrodynamics (MHD) simulations. According to the numerical tests for a wide range of flow and magnetic conditions, its reliability, efficiency, and accuracy have been successfully demonstrated.

- Robustness of SLAU2 against shock-anomalies (e.g., carbuncle phenomena) has been confirmed in the MHD-extended hypersonic flow test by the authors.
- The computational cost has been reduced for approximately 3% compared with HLLD (Harten-Lax-van_Leer with Discontinuities), a more expensive, 5-wave solver.
- Nevertheless, its solution qualities are almost equal to those of HLLD, as opposed to very diffused HLL solutions. For benchmark tests, detailed and important flow physics such as multidimensional shock/shock interactions have been successfully reproduced by SLAU2.
- SLAU2 exhibit slightly larger oscillations than HLLD did in a limited case. Although they appear to be acceptable, a hybridization with a 7-wave solver may suppress those oscillations, as conducted in our precedent work for one-dimensional MHD.

We presented a new carbuncle test and several well-known benchmark problems in two-dimensional MHD. All the results support efficacies of SLAU2 in MHD simulations, and the three-dimensional extension as a more realistic simulation is left as a future work.

Acknowledgments

This work was partially conducted while the first author (K. Kitamura) was visiting at Ulsan National Institute of Science and Technology (UNIST), Republic of Korea. We would like to express gratitude to UNIST for hosting the first author, and also to Yokohama National University, Japan, for financial support. The first author also thanks Dr. Takashi Minoshima at Japan Agency for Marine-Earth Science and Technology (JAMSTEC), Japan, and Mr. Tomohiro Mamashita at Yokohama National University for having valuable discussions, conducting the relevant simulations, and reporting the results. This work was supported by JSPS KAKENHI Grant Number JP19K04834. The work of Dongsu Ryu was supported by the NRF of Korea through grants 2016R1A5A1013277 and 2017R1A2A1A05071429.

References

[1] Esquivel, A., Raga, A. C., Cantó, J., Rodríguez-González, A., López-Cámara, D., Velázquez, P. F., and De Colle, F., "Model of Mira'sCometary Head/Tail Entering the Local Bubble," *Astrophysical Journal*, Vol. 725, 2010, pp. 1466–1475.

[2] Ohnishi, N., Kotake, K., and Yamada, S., "Numerical Analysis on Standing Accretion Shock Instability with Neutrino Heating in the Supernova Cores" *Astrophysical Journal*, Vol. 667, No. 1, 2007, pp.375-381.

[3] Hanawa, T., Mikami, H., Matsumoto, T., "Improving shock irregularities based on the characteristics of the MHD equations," *J. Comput. Phys.*, Vol. 227, 2008, pp.7952–7976.

[4] Poggie, J. and Gaitonde, D.V., "Magnetic Control of Flow Past a Blunt Body: Numerical Validation and Exploration," *Physics of Fluids*, Vol. 14, No. 1720, 2002, pp.1720-1731.

[5] ITER Physics Expert Groups on Confinement and Transport and Confinement Modelling and Database, "ITER Physics Basis", *Nuclear Fusion*, Vol.39, 1999, pp. 2137-2638.

[6] Loarte, A., Liu, F., Huijsmans, G. T. A., Kukushkin, A. S., and Pitts, R. A., "MHD stability of the ITER pedestal and SOL plasma and its influence on the heat flux width", *Journal of Nuclear Materials*, Vol. 463, 2015, pp. 401-405.

[7] van Leer, B., "Towards the ultimate conservative difference scheme. V. A second-order sequel to Godunov's method," *J. Comput. Phys.*, Vol. 32, No. 1, 1979, pp.101–136.

[8] Suresh, A., and Huynh, H.T., "Accurate Monotonicity-Preserving Schemes with Runge–Kutta Time Stepping", *J. Comput. Phys.*, Vol.136, 1997, pp.83–99.

[9] Roe, P.L., "Characteristic-based Schemes for the Euler Equations," *Ann. Rev. Fluid Mech.*, Vol.18, 1986, pp. 337-365.

[10]Roe, P.L., "Approximate Riemann Solvers, Parameter Vectors, and Difference Schemes," *J. Comput. Phys.*, Vol. 43, 1981, pp.357-372.

[11] Miyoshi, T., and Kusano, K., "A Multi-State HLL Approximate Riemann Solver for Ideal Magnetohydrodynamics," *J. Comput. Phys.*, Vol. 208, 2005, pp. 315–344.

[12] Kitamura, K., and Shima, E., "Towards Shock-Stable and Accurate Hypersonic Heating Computations: A New Pressure Flux for AUSM-family Schemes," *J. Comput. Phys.*, Vol.245, 2013, pp.62-83.

[13] Harten, A., Lax, P.D., and Van Leer, B., "On upstream differencing and Godunov-type schemes for hyperbolic conservation laws," *SIAM Reviews*, Vol. 25, No. 1, 1983, pp.35–61.

[14] Gottlieb S., and Shu, C.-W., "Total variation diminishing Runge–Kutta schemes", *Math. Comput.*, Vol. 67, 1998, pp.73–85.

[15] Dedner, A., Kemm, F., Kroner, D., Munz, C. D., Schnitzer, T., and Wesenberg, M., "Hyperbolic Divergence Cleaning

for the MHD Equations," *J. Comput. Phys.*, Vol. 175, 2002, pp. 645–673.

[16] Balsara, D.S., "Second-order-accurate schemes for magnetohydrodynamics with divergence-free reconstruction," *Astrophys. J. Suppl. Ser.*, Vol.151, 2004, pp.149–184.

[17] Balsara, D.S., and Spicer, D.S., "A Staggered Mesh Algorithm using High Order Godunov Fluxes to Ensure Solenoidal Magnetic Fields in Magnetohydrodynamics Simulation," *J. Comput. Phys.*, Vol.149, 1999, pp.270-292.

[18] Tóth, G., "The $\nabla \cdot B = 0$ Constraint in Shock-Capturing Magnetohydrodynamics Codes," *J. Comput. Phys.*, Vol. 161, 2000, pp. 605–652.

[19] Powell, K. G., Roe, P. L., Linde, T., Gombosi, T. I., and De Zeeuw, D. L., "A Solution-Adaptive Upwind Scheme for Ideal Magnetohydrodynamics," *J. Comput. Phys.*, Vol. 154, 1999, pp. 284–309.

[20]Kitamura, K., Shima, E., Fujimoto, K., and Wang, Z.J.: Performance of Low-Dissipation Euler Fluxes and Preconditioned LU-SGS at Low Speeds, *Communi. in Comput. Phys.*, Vol.10, No.1, 2011, pp.90-119.

[21] Pandolfi, M. and D'Ambrosio, D.: Numerical Instabilities in Upwind Methods: Analysis and Cures for the "Carbuncle" Phenomenon, *J. Comput. Phys.*, Vol. 166, No. 2, 2001, pp.271-301.

[22] Chauvat, Y., Moschetta, J. M., and Gressier, J., "Shock Wave Numerical Structure and the Carbuncle Phenomenon," *International Journal for Numerical Methods in Fluids*, Vol. 47, Nos. 8–9, 2005, pp. 903–909.

[23] Dumbser, M., Moschetta, J. M., and Gressier, J., "A Matrix Stability Analysis of the Carbuncle Phenomenon," *J. Comput. Phys.*, Vol. 197, No. 2, 2004, pp. 647–670.

[24] Quirk, J. J., "A Contribution to the Great Riemann Solver Debate," *International Journal for Numerical Methods in Fluids*, Vol. 18, No. 6, 1994, pp. 555–574.

[25] Kitamura, K., Roe, P., and Ismail, F., "Evaluation of Euler Fluxes for Hypersonic Flow Computations," *AIAA Journal*, Vol. 47, 2009, pp.44-53.

[26] Kitamura, K., Shima, E., and Roe, P., "Carbuncle Phenomena and Other Shock Anomalies in Three Dimensions," *AIAA Journal*, Vol. 50, No. 12, 2012, pp. 2655–2669.

[27] Brio, M., and Wu, C. C., "An Upwind Differencing Scheme for the Equations of Ideal Magnetohydrodynamics," *J. Comput. Phys.*, Vol. 75, 1988, pp. 400–422.

[28] Ryu, D. S., and Jones, T. W., "Numerical Magnetohydrodynamics in Astrophysics: Algorithm and Test for One-Dimensional Flow," *Astrophysical Journal*, Vol. 442, 1995, pp. 228–258.

[29] Roe, P. L., and Balsara, D. S., "Notes on the Eigensystem of Magnetohydrodynamics," *SIAM J. Appl. Math.*, Vol. 56, 1996, pp. 57–67.

[30] Cargo, P., Gallice, G., "Roe Matrices for Ideal MHD and Systematic Construction of Roe Matrices for Systems of Conservation Laws," *J. Comput. Phys.*, Vol. 136, 1997, pp.446-466.

[31] Balsara, D.S., Linearized Formulation of the Riemann Problem for Adiabatic and Isothermal Magnetohydrodynamics, *Ap.J. Supp.*, Vol. 116, 1998, pp.119-131.

[32] Dumbser, M., and D.S. Balsara, "A new efficient formulation of the HLLEM Riemann solver for general conservative and non-conservative hyperbolic systems," *J. Comput. Phys.,* Vol.304, 2016, pp.275–319.

[33] Liou, M.S., "Mass flux schemes and connection to shock instability," *J. Comput. Phys,.* Vol. 160, 2000, pp.623–648.

[34] Matsumoto, Y., Asahina, Y., Kudoh, Y., Kawashima, T., Matsumoto, J., Takahashi, H.R., Minoshima, T., Zenitani, S., Miyoshi, T., and Matsumoto, R., "Magnetohydrodynamic Simulation Code CANS+: Assessments and Applications," *Publ. Astron. Soc. Japan*, Vol. 71, Issue 4, 2019, p.83, doi:10.1093/pasj/psz064

[35] Stone, J.M., Gardiner, T.A., Teuben, P., Hawley, J.F., and Simon, J.B., "ATHENA: A New Code for Astrophysical MHD," *The Astrophysical Journal Supplement Series*, Vol. 178, No.1, 2008, pp.137-177.

[36] Minoshima, T., Miyoshi, T., and Matsumoto, Y., "A high-order weighted finite difference scheme with a multi-state approximate Riemann solver for divergence-free magnetohydrodynamic simulations", *Ap.J. Supp*, Vol. 242, No. 2, 2019.

[37] Kitamura, K. and Balsara, D.S.: "Hybridized SLAU2–HLLI and hybridized AUSMPW+–HLLI Riemann solvers for accurate, robust, and efficient magnetohydrodynamics (MHD) simulations, part I: one-dimensional MHD," *Shock Waves*, Vol. 29, 2019, pp.611-627.

[38] Xisto, C.M., Páscoa1, J.C., and Oliveira, P.J., "A Pressure-Based High Resolution Numerical Method for Resistive MHD," *J. Comput. Phys.*, Vol. 275, 2014, pp.323–345.

[39] Han, S.H., Lee, J.I., and Kim, K.H., "Accurate and Robust Pressure Weight Advection Upstream Splitting Method for Magnetohydrodynamics Equations," *AIAA Journal*, Vol. 47, No. 4, 2009, pp. 970-981.

[40] Shen, Y., Zha, G., Huerta, M.A., "E-CUSP Scheme for the Equations of Ideal Magnetohydrodynamics with High Order WENO Scheme," *J. Comput. Phys.*, Vol. 231, 2012, pp.6233-6247.

[41] Li, S., "An HLLC Riemann Solver for Magnetohydrodynamics," *J. Comput. Phys.*, Vol. 203, 2005, pp. 344–357.

[42] Gurski, K.F., "An HLLC-Type Approximate Riemann Solver for Ideal Magnetohydrodynamics," *SIAM J. Sci. Comput.*, Vol. 25, No.6, 2004, pp.2165–2187.

[43] Van Leer, B., "Flux-vector splitting for the Euler equations," *Lect. Notes Phys.*, Vol. 170, 1982, pp.507–512.

[44] Kim, K. H., Kim, C., and Rho, O. H., "Methods for the Accurate Computations of Hypersonic Flows: I. AUSMPW+ Scheme," *J. Comput. Phys.*, Vol. 174, 2001, pp. 38–80.

[45] Kitamura, K., Shima, E., Nakamura, Y., and Roe, P., "Evaluation of Euler fluxes for hypersonic heating computations," *AIAA J.*, Vol. 48, No. 4, 2010, pp.763–776.

[46] Zha, G.-C., Shen, Y., Wang, B., "An improved low diffusion E-CUSP upwind scheme", *Computers & Fluids*, Vol. 48, 2011, pp.214–220

[47] Kitamura, K., "Assessment of SLAU2 and Other Flux Functions with Slope Limiters in Hypersonic Shock-Interaction Heating," *Computers & Fluids*, Vol.129, 2016, pp.134-145.

[48]Weiss, J.M. and Smith, W.A.: Preconditioning Applied to Variable and Constant Density Flows, *AIAA Journal*, Vol. 33, No.11, 1995, pp. 2050-2057.

[49] Liu, Y., and Vinokur, M., "Upwind Algorithms for General Thermo-Chemical Nonequilibrium Flows," AIAA Paper 89-0201, 1989.

[50] Toro E.F., Spruce M., and Speares W., "Restoration of the contact surface in the HLL Riemann solver," *Shock Waves*, Vol. 4, 1994, pp.25–34.

[51] Rusanov, V.V., "Calculation of Interaction of Non-Steady Shock Waves with Obstacles," *Journal of Computational and Mathematical Physics USSR*, Vol. 1, 1961, pp.267–279.

[52] Janhunen, P., "A Positive Conservative Method for Magnetohydrodynamics Based HLL and Roe Methods," *J. Comput. Phys,*, Vol. 160, 2000, pp. 649–661.

[53] Sanders, R., Morano, E., and Druguetz, M. C., "Multidimensional Dissipation for Upwind Schemes: Stability and Applications to Gas Dynamics," *J. Comput. Phys,*, Vol. 145, No. 2, 1998, pp. 511–537.

[54] Shima, E., and Kitamura, K., "Multidimensional numerical noise from captured shockwave and its cure," *AIAA J.*, Vol. 51, 2013, pp.992–998.

[55] Hashimoto, A., Murakami, K., Aoyama, T., Ishiko, K., Hishida, M., Sakashita, M., and Lahur, P., "Toward the Fastest Unstructured CFD Code 'FaSTAR,' " AIAA-2012-1075, 2012.

[56] Kitamura, K., Fujimoto, K., Shima, E., Kuzuu, K., and Wang, Z.J., "Validation of an arbitrary unstructured CFD code for aerodynamic analyses," *Trans. Jpn. Soc. Aeronaut. Space Sci.*, Vol. 53, 2011, pp.311–319.

[57] Molina, E., Zhou, B.Y., Alonso, J.J., Righi, M., and Silva, R.G., "Flow and Noise Predictions Around Tandem Cylinders using DDES approach with SU2", AIAA 2019-0326, AIAA Scitech 2019 Forum, 7-11 January 2019, San Diego, California.

[58] Brown, B.P., Vasil, G.M., and Zweibel, E.G., "Energy Conservation and Gravity Waves in Sound-Proof Treatments of Stellar Interiors. Part I. Anelastic Approximations," *Astrophysical Journal*, 756:109 (20pp), 2012.

[59] MacGregor, K. B. and Rogers, T. M., "Reflection and Ducting of Gravity Waves Inside the Sun," *Solar Physics*, Vol. 270, Issue 2, 2011, pp 417–436.

[60] Brun, A.S., Miesch, M.S., and Toomre, J., "Modeling the Dynamical Coupling of Solar Convection with the Radiative Interior," *Astrophysical Journal*, 742:79 (20pp), 2011

[61] Stix, M., "The Sun: an introduction," 2nd edn., Astronomy and astrophysics library (Berlin: Springer), ISBN: 3-540-20741-4, 2004.

[62] Liou, M.-S., "A Sequel to AUSM, Part II: AUSM$^+$-up for All Speeds," *J. Comput. Phys.*, Vol. 214, 2006, pp.137-170.

[63] Ryu, D., Jones, T.W., and Frank, A., "Numerical magnetohydrodynamics in astrophysics: Algorithm and tests for multi-dimensional flow", *The Astrophysical Journal*, Vol. 452, 1995, pp.785-796.

[64] Barth, T. J., "Some Notes on Shock-Resolving Flux Functions Part 1: Stationary Characteristics," NASA TM-101087, 1989.

[65] Orszag A., and Tang, C. M., "Small-Scale Structure of Two-Dimensional Magnetohydrodynamic Turbulence," *Journal of Fluid Mechanics*, Vol. 90, 1979, pp. 129–143.

[66] Gardiner, T.A., and Stone, J.M., "An unsplit Godunov method for ideal MHD via constrained transport", *J. Comput. Phys,*, Vol.205, 2005, pp.509–539.

[67] Londrillo, P., and Del Zanna, L., "High-Order Upwind Schemes for Multidimensional Magnetohydrodynamics," *The Astrophysical Journal*, Vol. 530, No. 1, 2000, pp.508-524.

[68] Dai, W. and Woodward, P.R, "On the Divergence-free Condition and Conservation Laws in Numerical Simulations for Supersonic Magnetohydrodynamical Flows" *The Astrophysical Journal*, Vol. 494, 1998, pp. 317-335.

[69] Miura, A., and Pritchett, P. L., "Nonlocal Stability Analysis of the MHD Kelvin-Helmholtz Instability in a Compressible Plasma" *J. Geophys. Res.*, Vol. 87, 1982, pp.7431-7444. doi: 10.1029/JA087iA09p07431

[70] CANS+ web site, http://www.astro.phys.s.chiba-u.ac.jp/cans/doc/application_kh.html (Accessed on Oct-01-2019)

[71] Tzeferacos, P., Fatenejad, M., Flocke, N., Graziani, C., Gregori, G., Lamb, D.Q., Lee, D., Meinecke, J., Scopatz, A., and Weide, K., "FLASH MHD Simulations of Experiments that study Shock-Generated Magnetic Fields," *High Energy Density Physics*, Vol. 17, Part A, 2015, pp.24–31.

[72] Mignone, A., Bodo, G., Massaglia, S., Matsakos, T., Tesileanu, O., Zanni, C., Ferrari, A., "PLUTO: a Numerical Code for Computational Astrophysics," arXiv:astro-ph/0701854 (accessed on Sep-19-2017) (2007)

[73] Linde, T, "A practical, general‐purpose, two‐state HLL Riemann solver for hyperbolic conservation laws," *Int. J. Numer. Meth. Fluids*, Vol.40, 2002, pp.391‐402. DOI: 10.1002/fld.312

Appendix A: HD Blast Wave

This problem has a setup very similar to "4.4 MHD Blast Wave" but *without* the magnetic field.

- $(\rho, u, v, w, p, B_x, B_y, B_z) = (1, 0, 0, 0, 1000, 0, 0, 0)$ inside a circle with 0.1 radius
- $(\rho, u, v, w, p, B_x, B_y, B_z) = (1, 0, 0, 0, 0.1, 0, 0, 0)$ elsewhere

with $\gamma = 5/3$. The solutions of SLAU2 and HLLD on 256 x 256 uniform cells are shown in Fig. A1, which demonstrates the SLAU2's smoother solution than HLLD which exhibit a zigzag-shaped shock profile.

Figures

a) 7-wave solvers (Roe, HLLI)

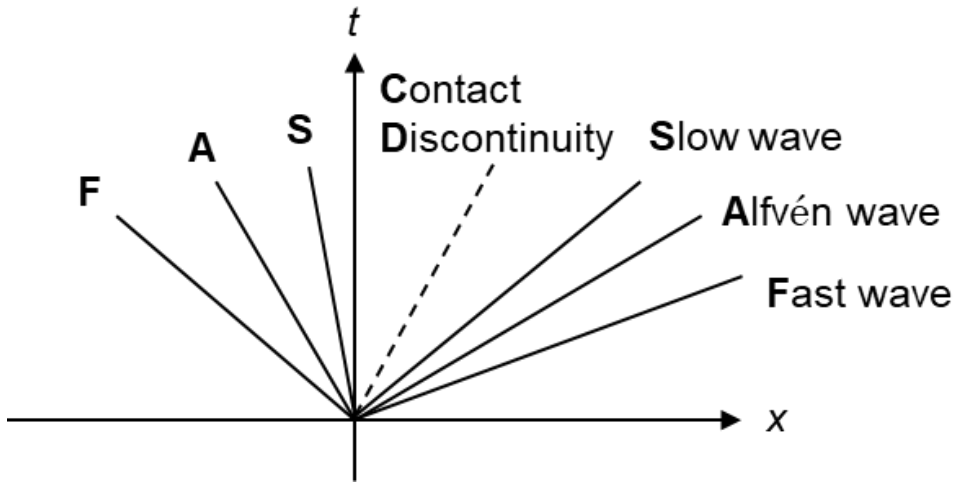

b) 5-wave solver (HLLD)

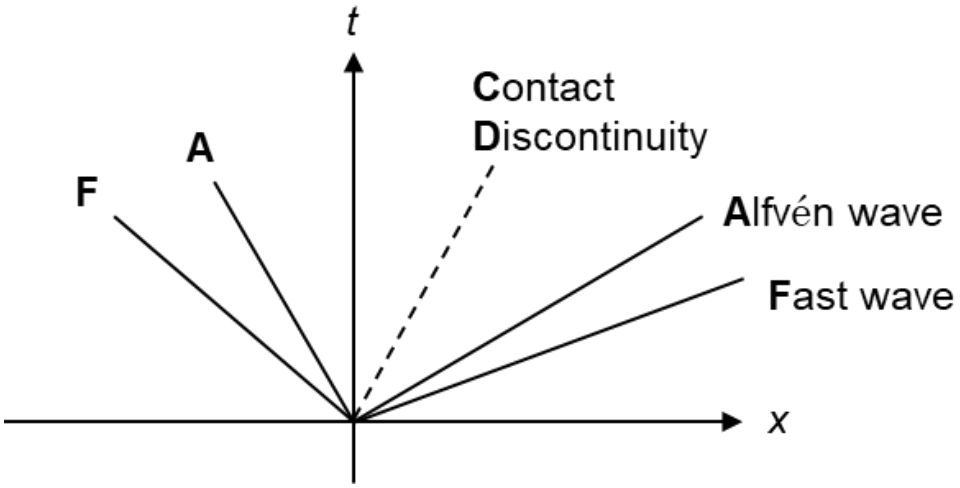

Fig. 1 Numerical Flux Functions in MHD; (a) 7-wave solvers (Roe, HLLI), (b) 5-wave solver (HLLD), (c) 3-wave solvers (SLAU2, AUSMPW+, E-CUSP, HLLC), and (d) 2-wave solver (HLL), continued.

c) 3-wave solvers (SLAU2, AUSMPW+, E-CUSP, HLLC)

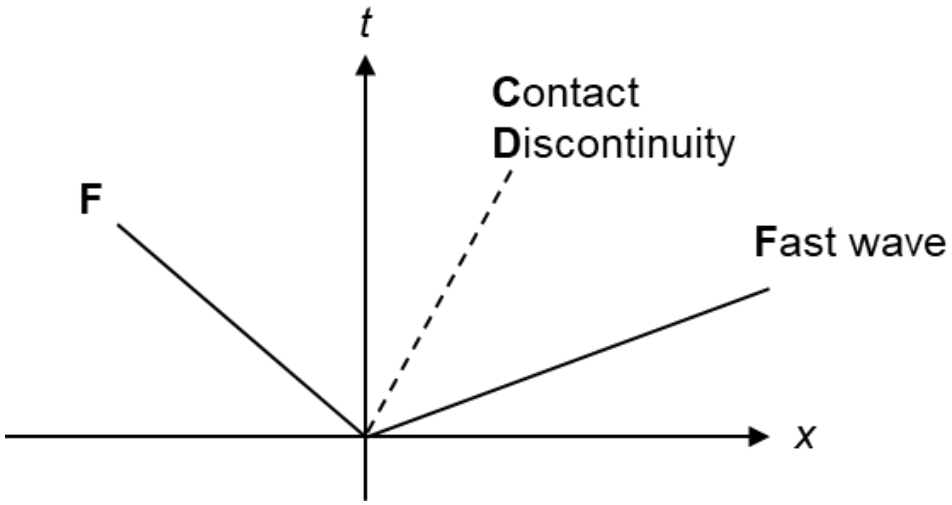

d) 2-wave solver (HLL)

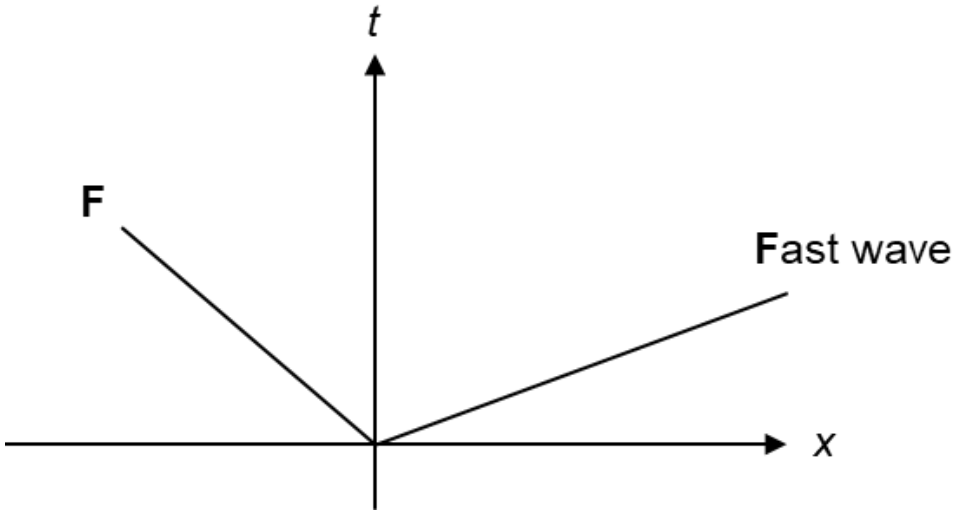

Fig. 1 Numerical Flux Functions in MHD; (a) 7-wave solvers (Roe, HLLI), (b) 5-wave solver (HLLD), (c) 3-wave solvers (SLAU2, AUSMPW+, E-CUSP, HLLC), and (d) 2-wave solver (HLL), concluded.

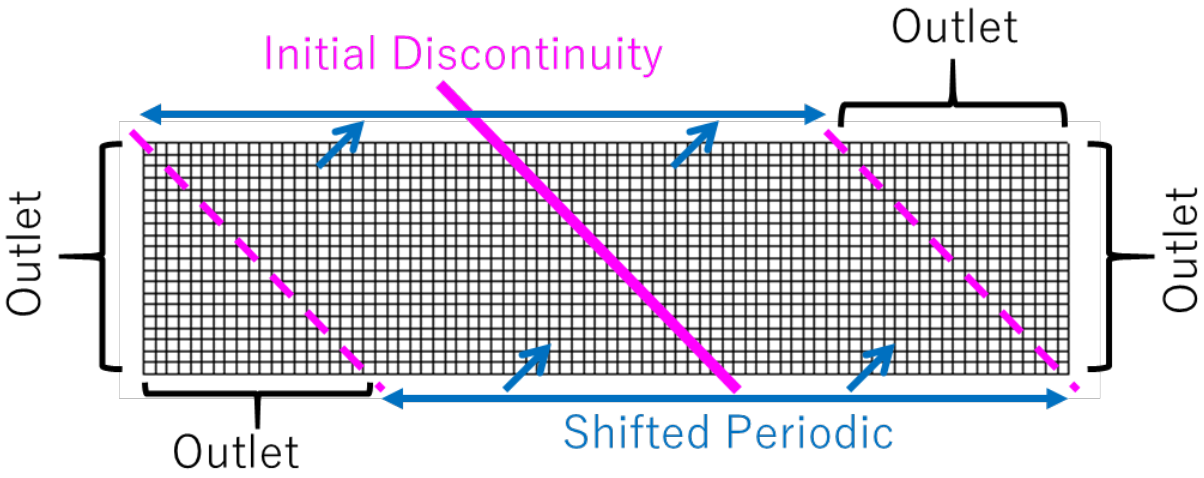

Fig. 2 2D-Extended Ryu-Jones Shocktube: Grid (every five lines are displayed) and Boundary Conditions.

a)

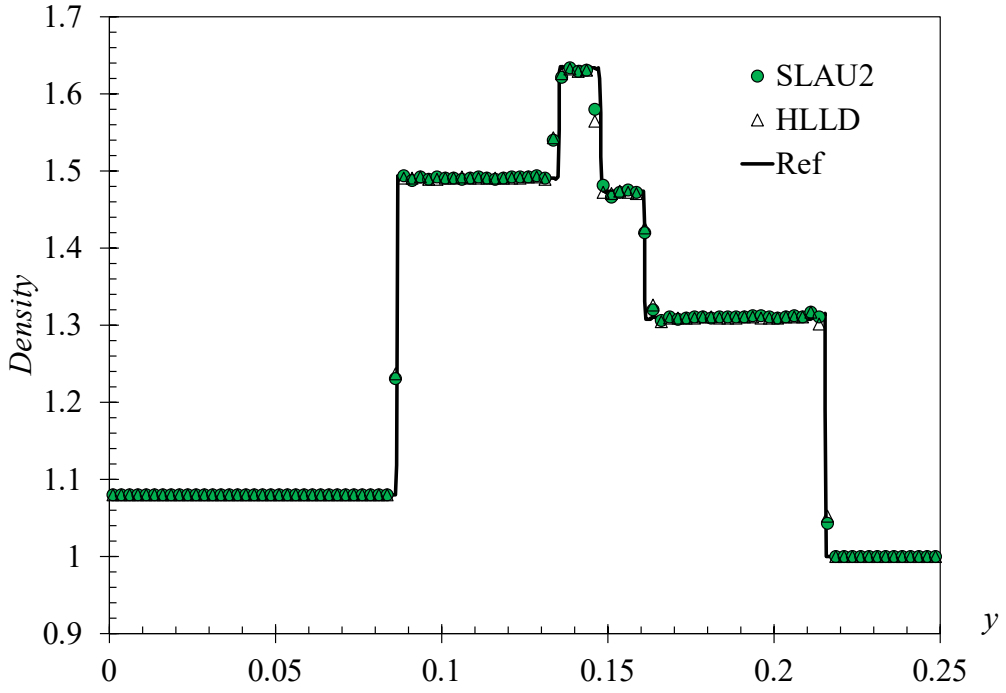

b)

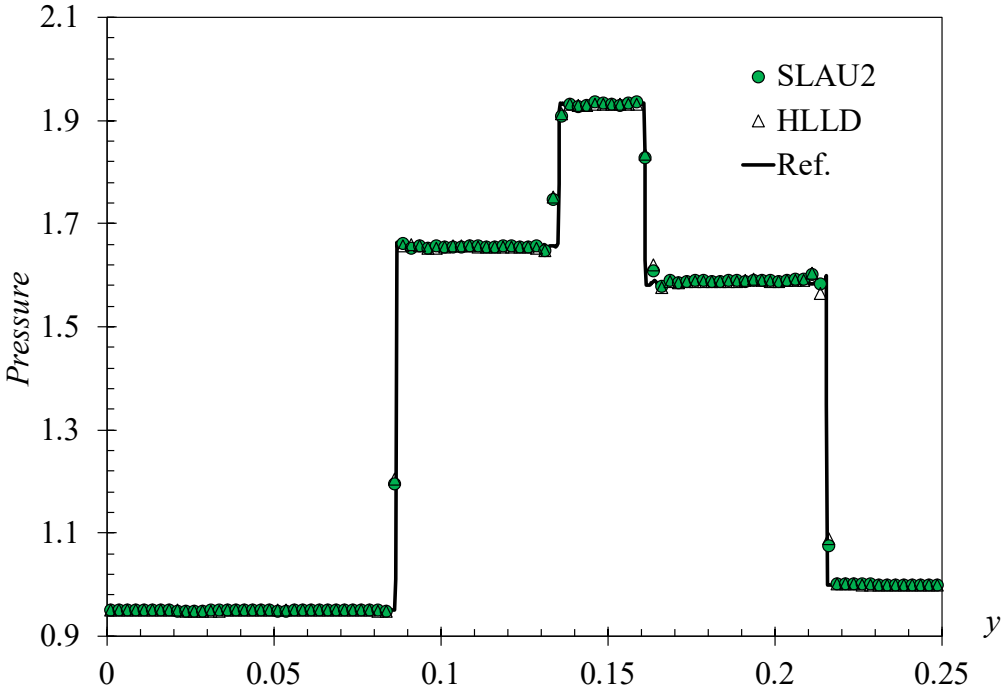

Fig. 3 2D-Extended Ryu-Jones Shocktube (400x100 cells), profiles along *x*-*y* =0.75 line; (a) density, and (b) pressure.

a)

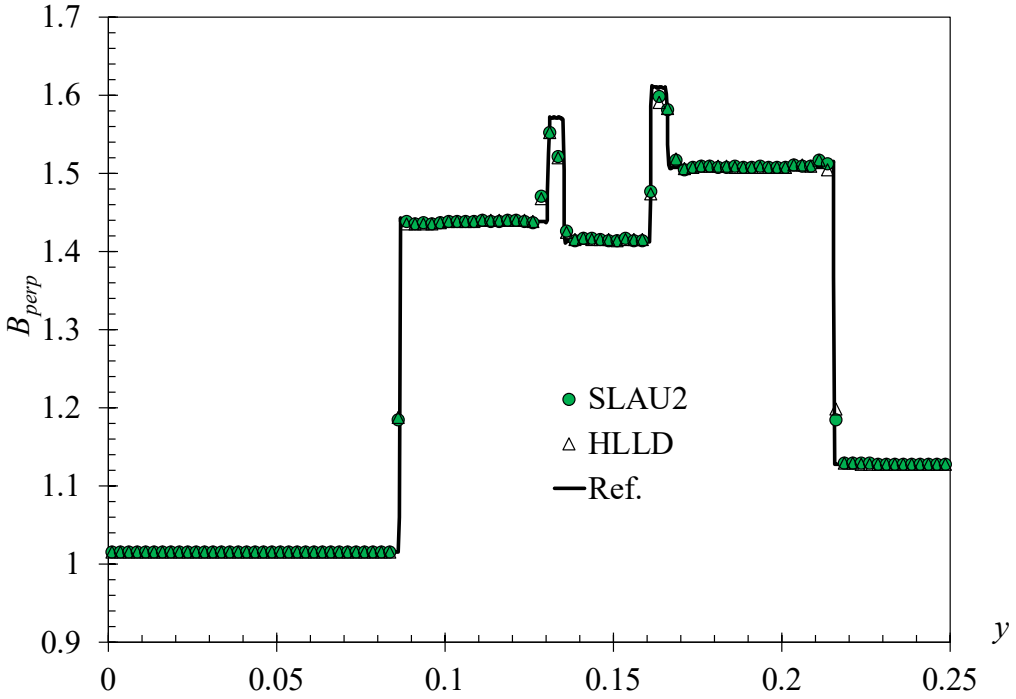

b)

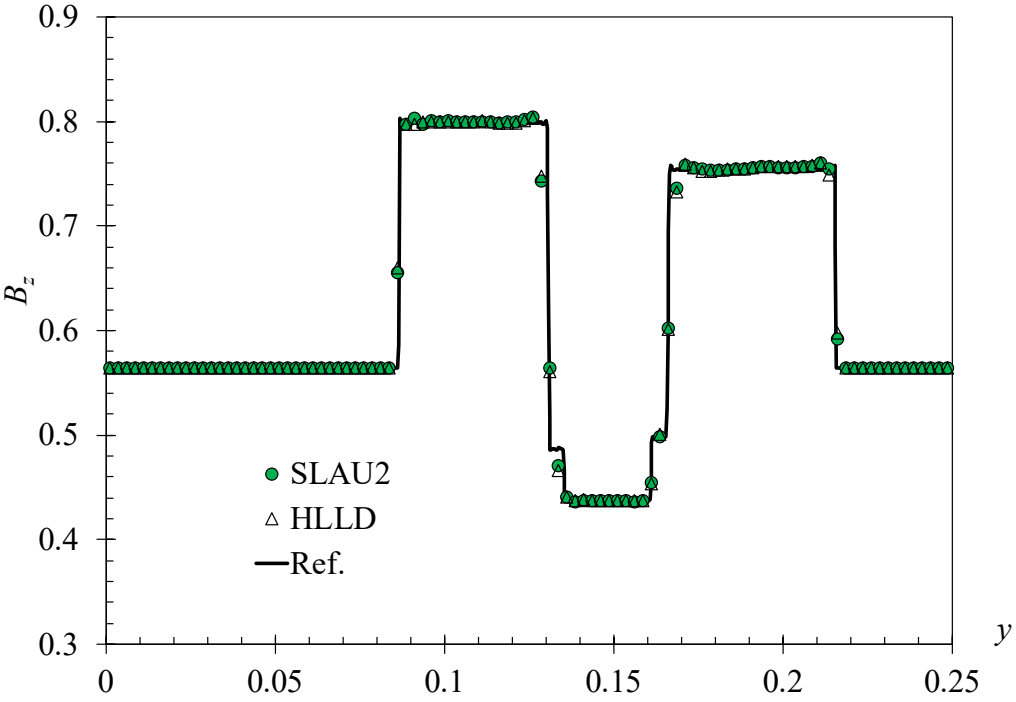

Fig. 4 2D-Extended Ryu-Jones Shocktube (400x100 cells), profiles along x-y =0.75 line; (a) $B_{perp} = (-B_x + B_y)\ /2^{0.5}$, and (b) B_z.

a) Grid, Initial Conditions, and Boundary Conditions

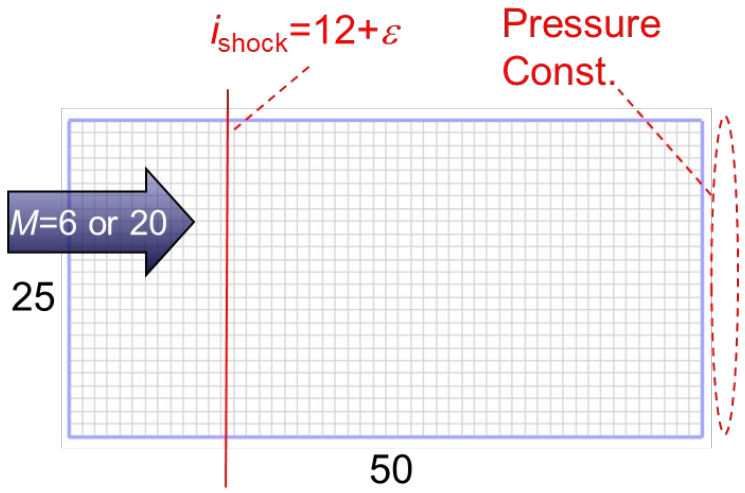

b) Initial Shock Location Parameter ε

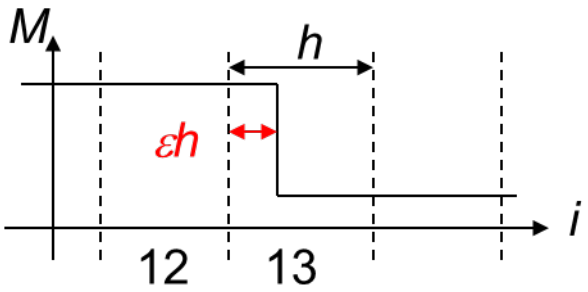

ε = 0.0, 0.1, …, 0.9
(Shock Location Parameter)

Fig. 5 MHD Carbuncle Test Setup, (a) Grid, Initial Conditions, and Boundary Conditions, (b) Initial Shock Location Parameter ε.

a) SLAU2, ε=0.0

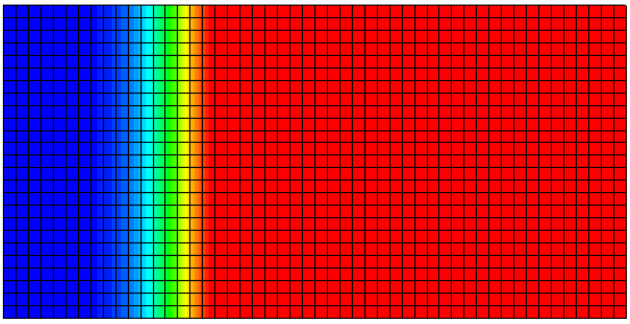

b) SLAU2, ε=0.5

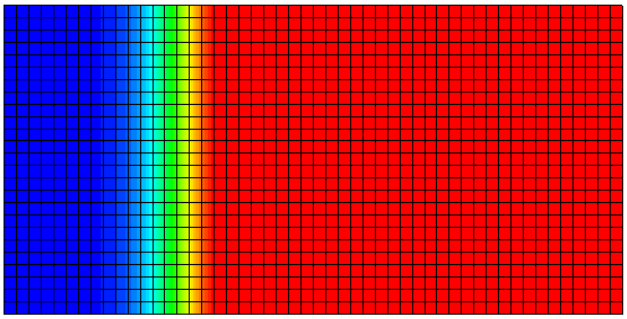

c) HLLD, ε=0.0

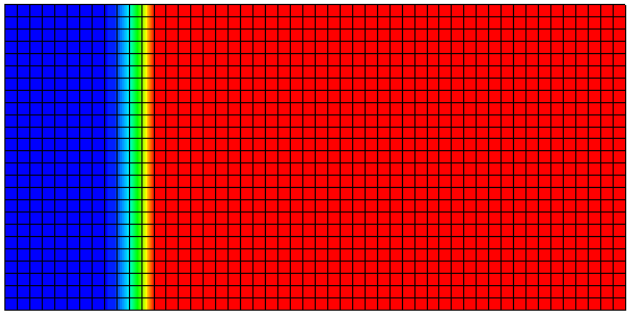

d) HLLD, ε=0.5

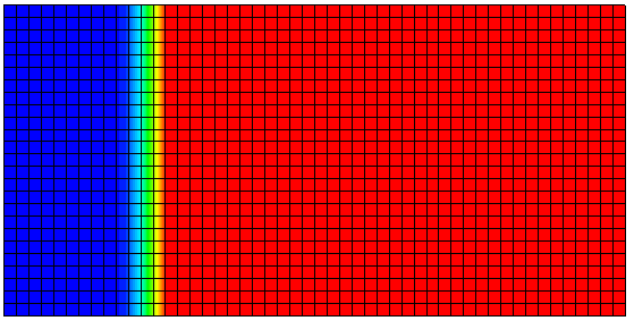

Fig. 6 ~~SLAU2~~ Solutions of MHD Carbuncle Test (Density) at Mach 20, (a) SLAU2, ε=0.0, (b) SLAU2, ε=0.5, (c) HLLD, ε=0.0, and (d) HLLD, ε=0.5.

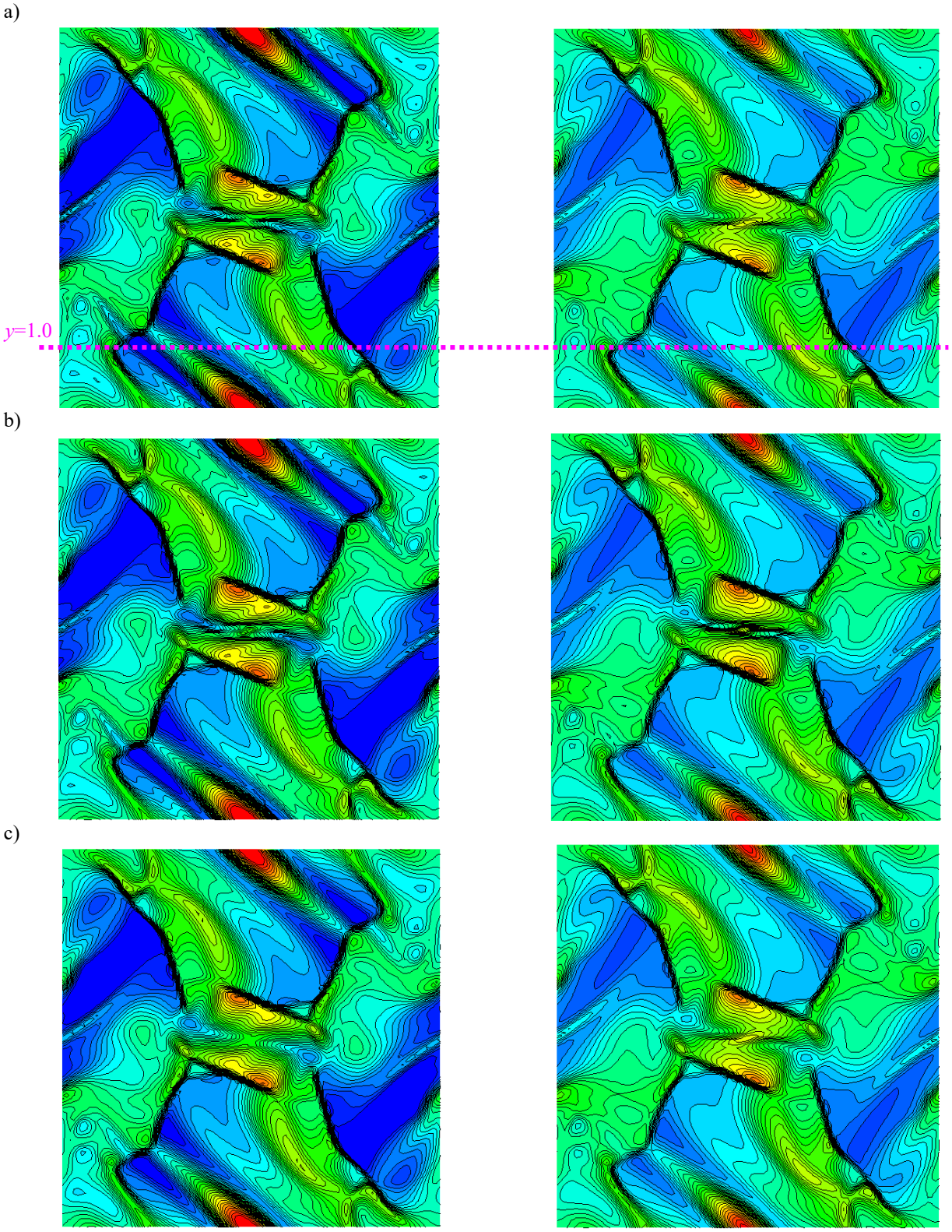

Fig. 7 Orzag-Tang Vortex Problem, (left) density, (right) pressure; (a)SLAU2, (b) HLLD, and (c) HLL.

a)

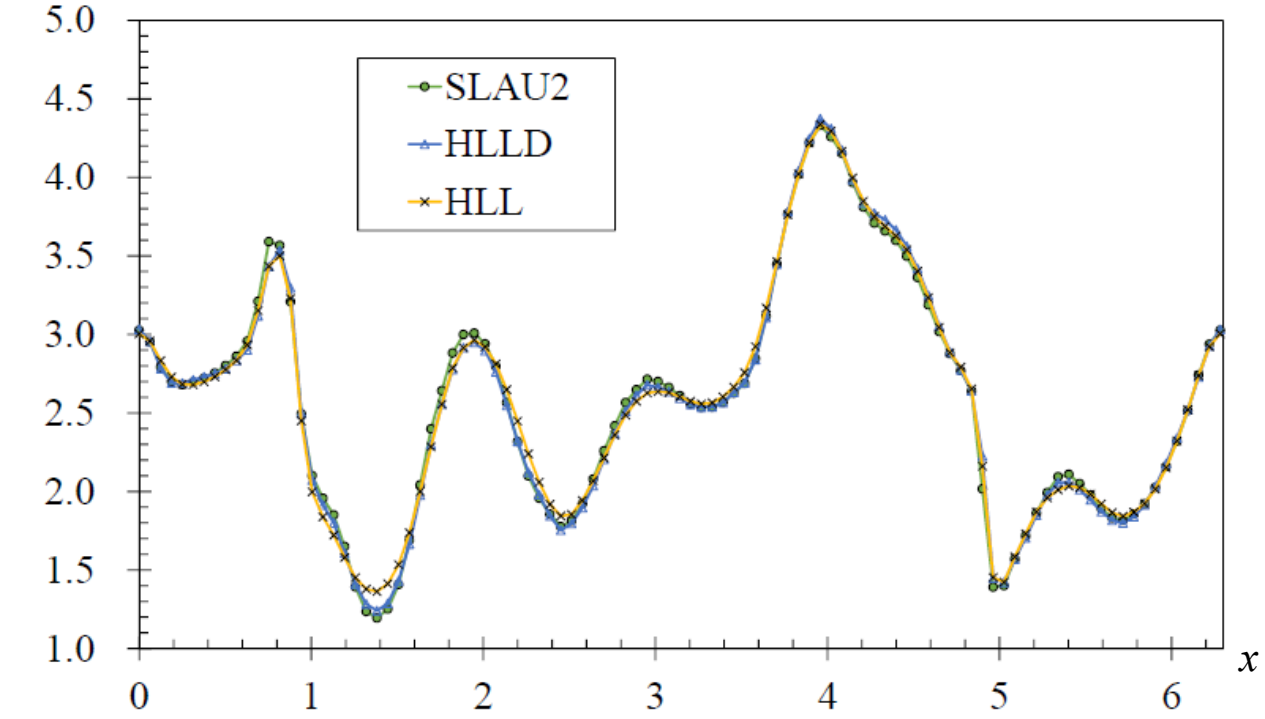

b)

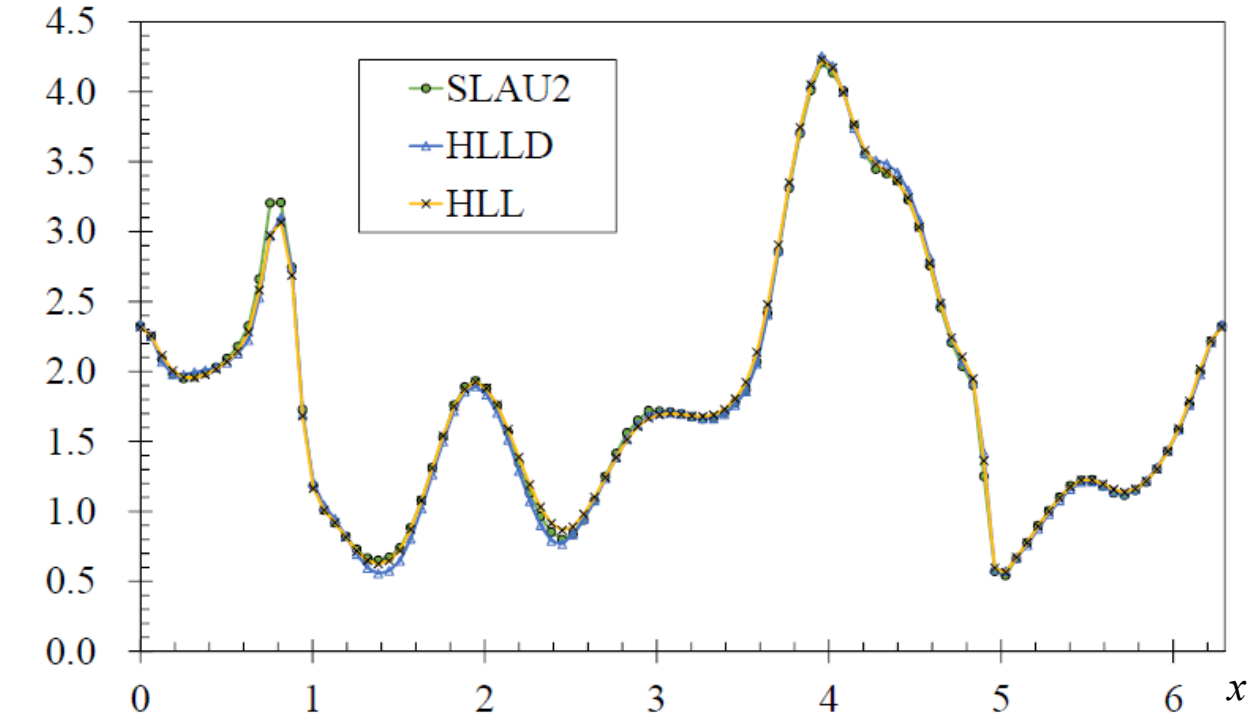

Fig. 8 Orzag-Tang Vortex Problem, profiles along y=1 line; (a) density, (b) pressure.

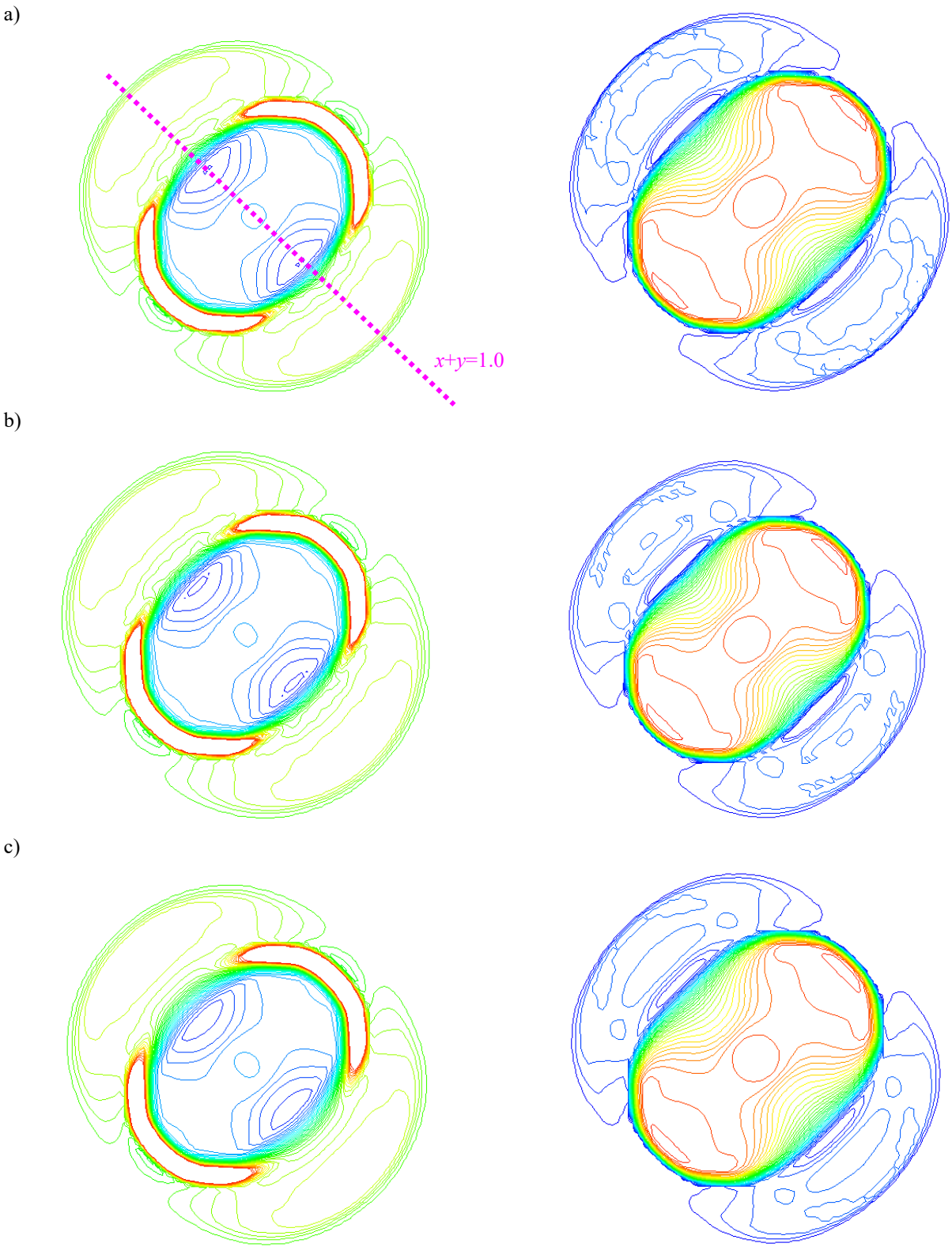

Fig. 9 MHD Blast Wave Problem (β=0.001), (left) density in logarithmic scale, (right) pressure in logarithmic scale; (a) SLAU2, (b) HLLD, and (c) HLL.

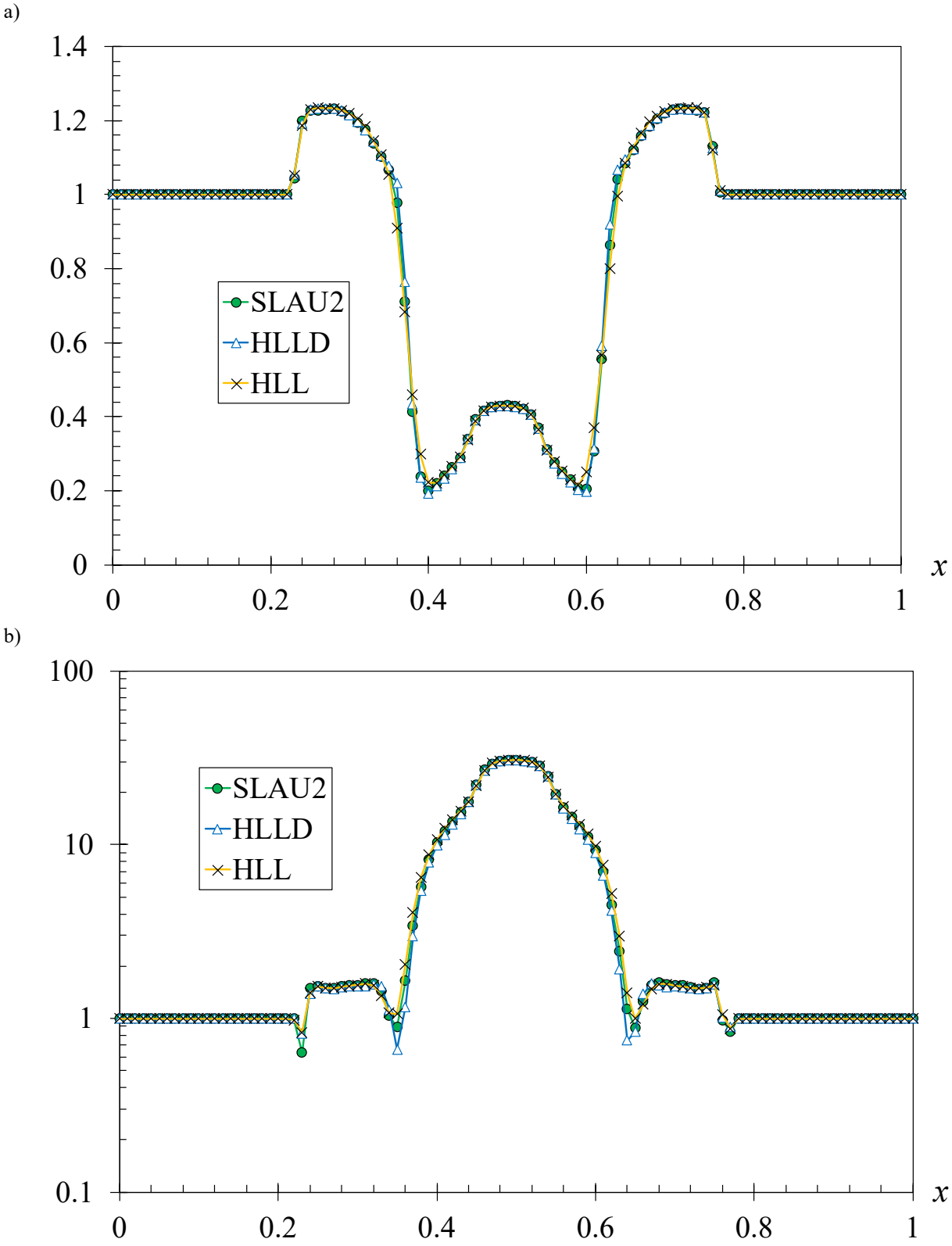

Fig. 10 MHD Blast Wave Problem (β=0.001), profiles along x+y=1 line; (a) density, (b) pressure.

a)

b)

c)

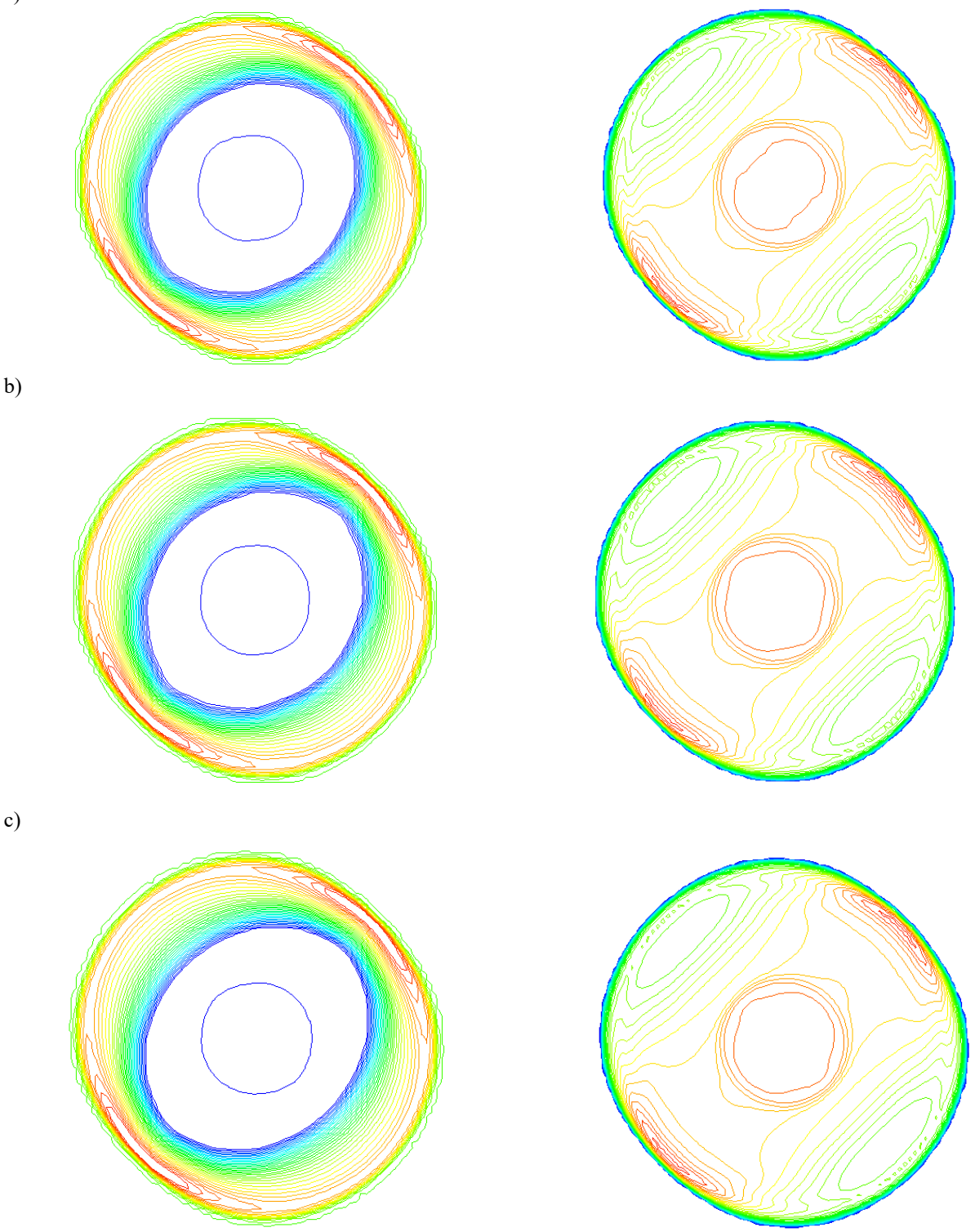

Fig. 11 MHD Blast Wave Problem (β=0.004), (left) density in logarithmic scale, (right) pressure in logarithmic scale; (a) SLAU2, (b) HLLD, and (c) HLL.

a)

b)

c)

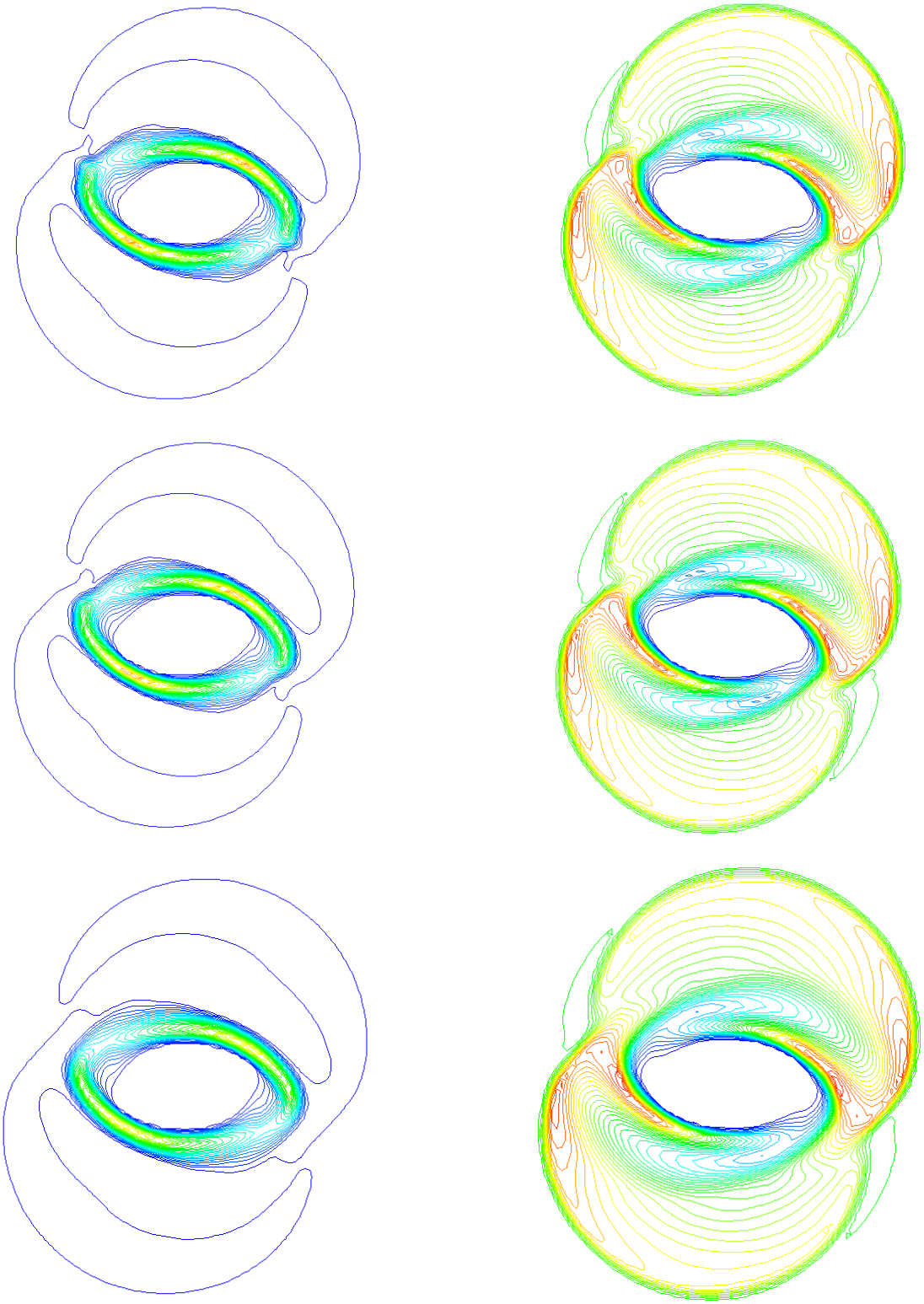

Fig. 12 MHD Rotor Problem (100x100 cells), (left) density, (right) pressure; (a) SLAU2, (b) HLLD, and (c) HLL.

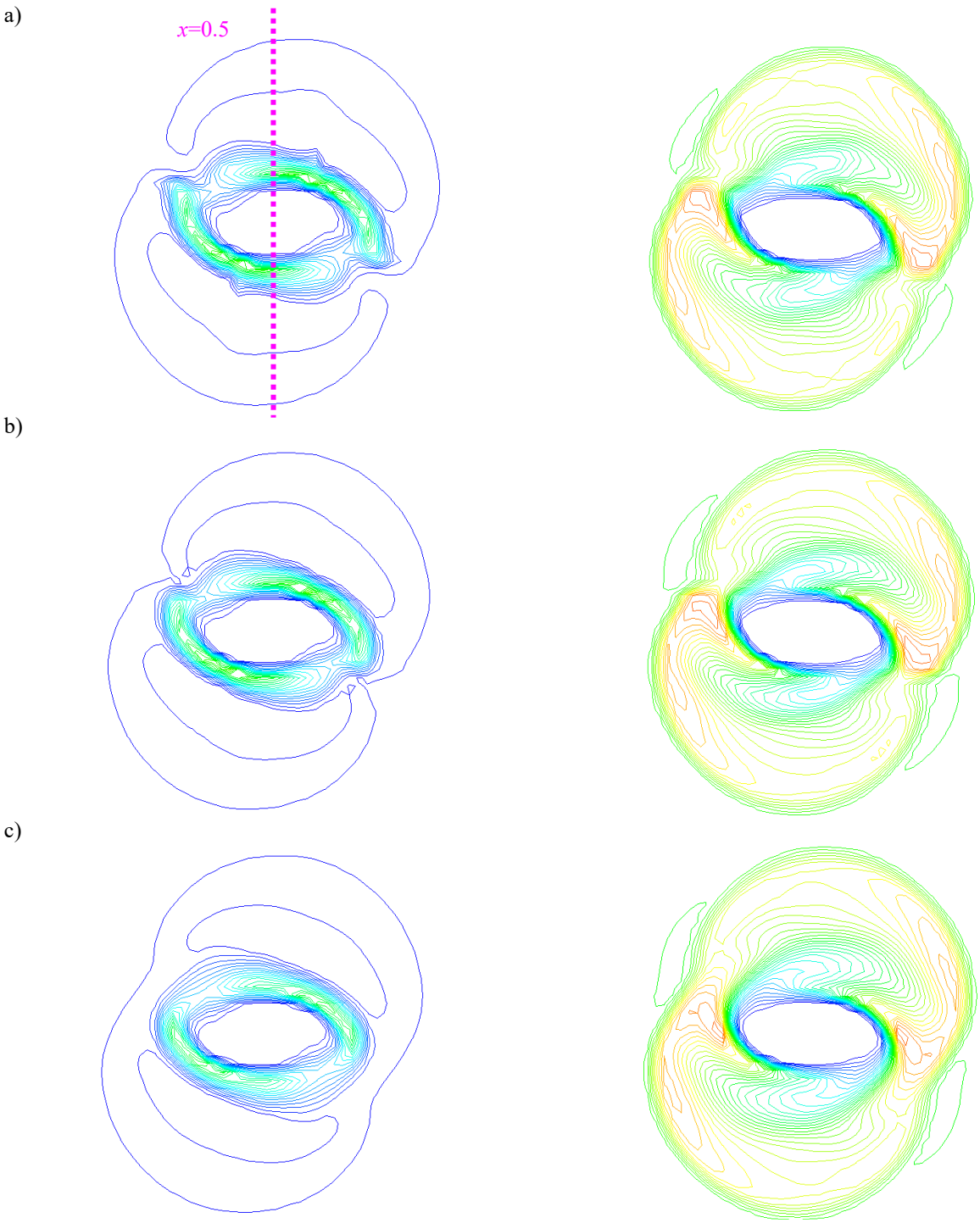

Fig. 13 MHD Rotor Problem (50x50 cells), (left) density, (right) pressure; (a) SLAU2, (b) HLLD, and (c) HLL.

a)

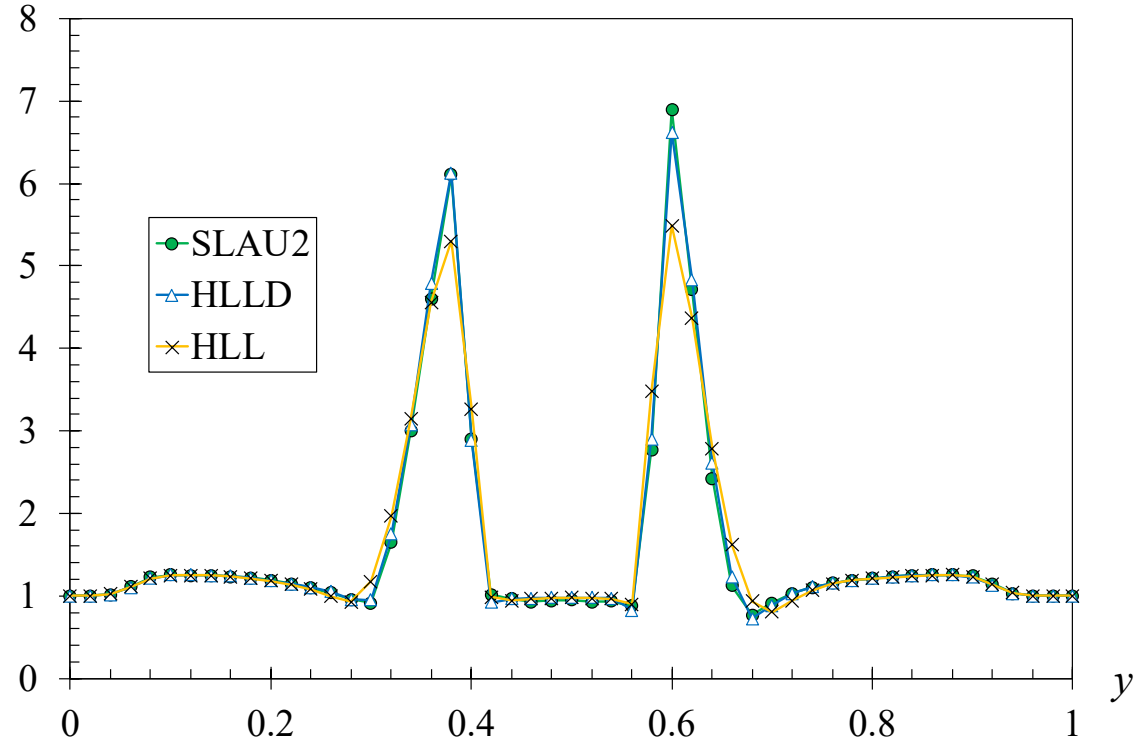

b)

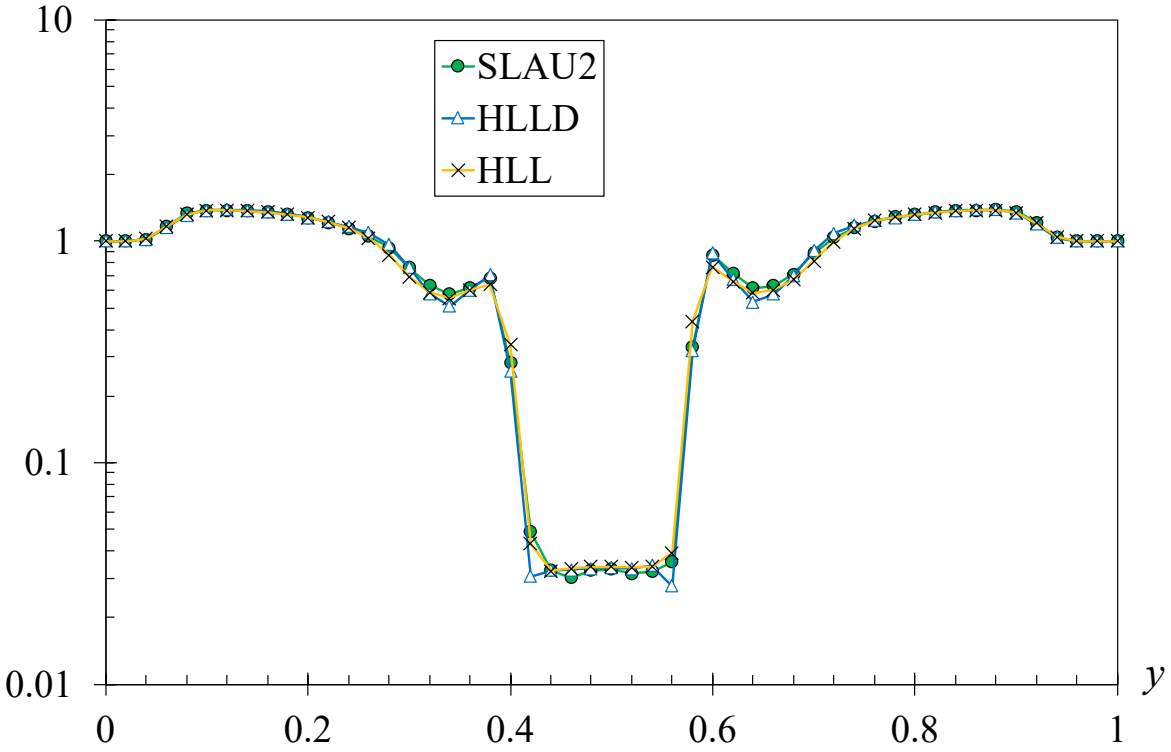

Fig. 14 MHD Rotor Problem (50x50 cells), profiles along x =0.5 line; (a) density, (b) pressure.

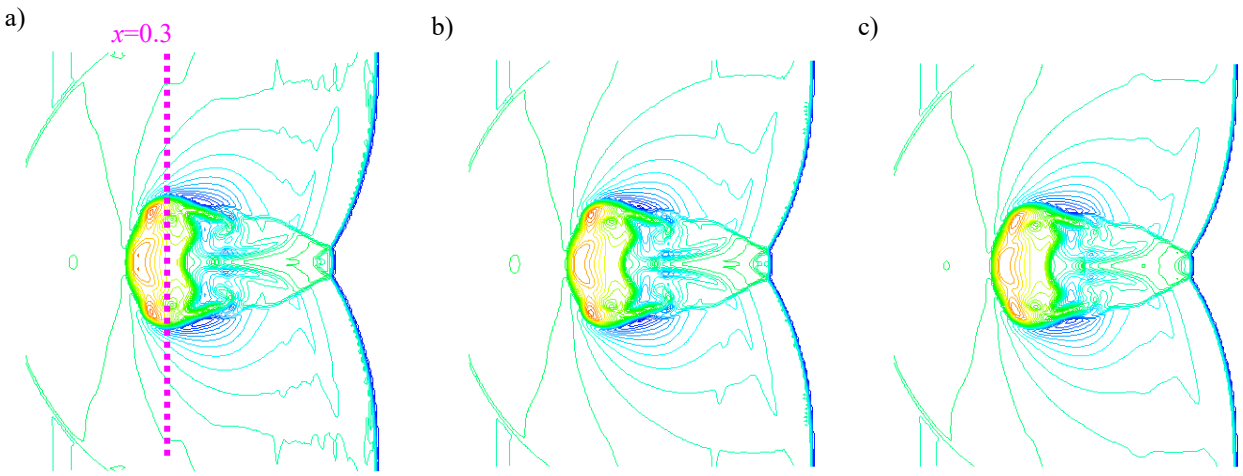

Fig. 15 MHD Shock/Cloud Interaction Problem (200x200 cells), density; (a) SLAU2, (b) HLLD, and (c) HLL.

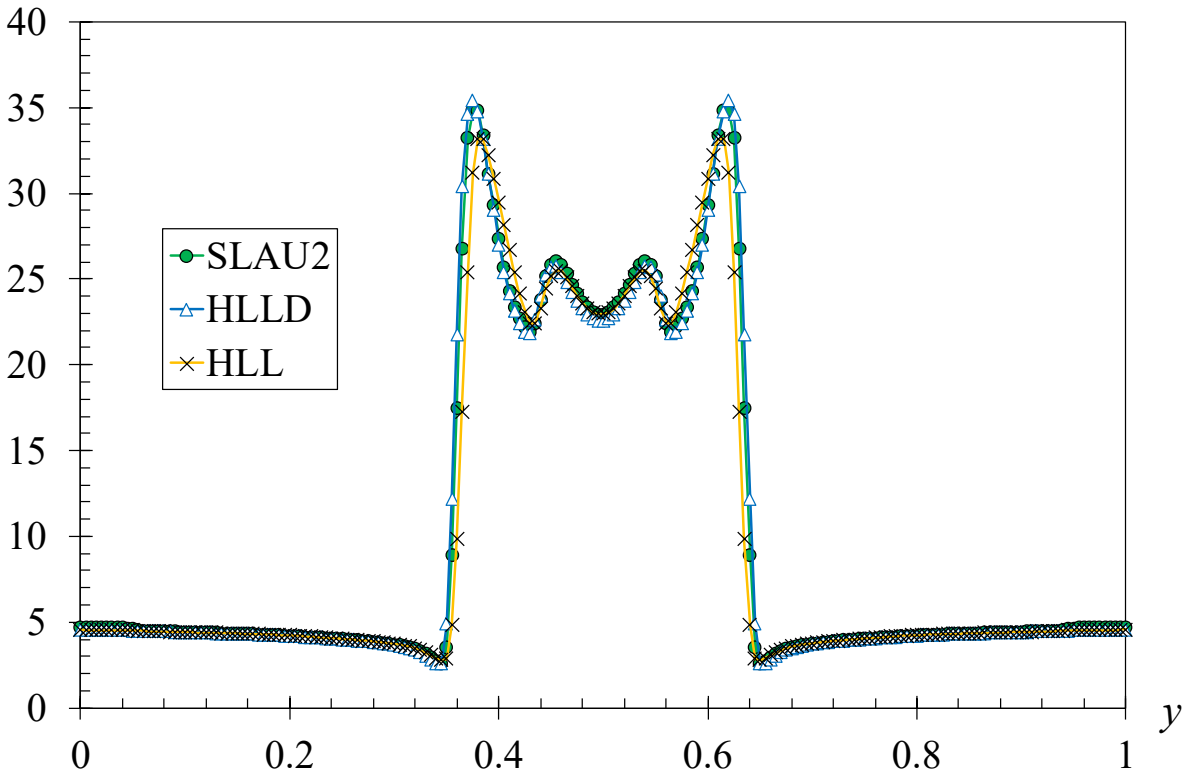

Fig. 16 MHD Shock/Cloud Interaction Problem, density profiles along x =0.3 line.

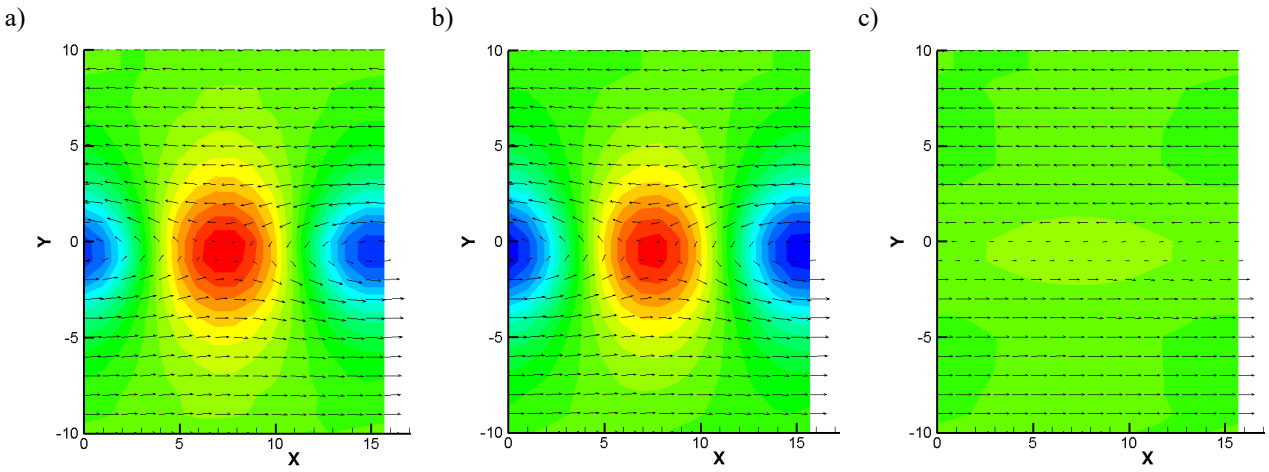

Fig. 17 Early Stage of Kelvin-Helmholtz Instability (16x20 cells), pressure with velocity vectors; (a) SLAU2, (b) HLLD, and (c) HLL.

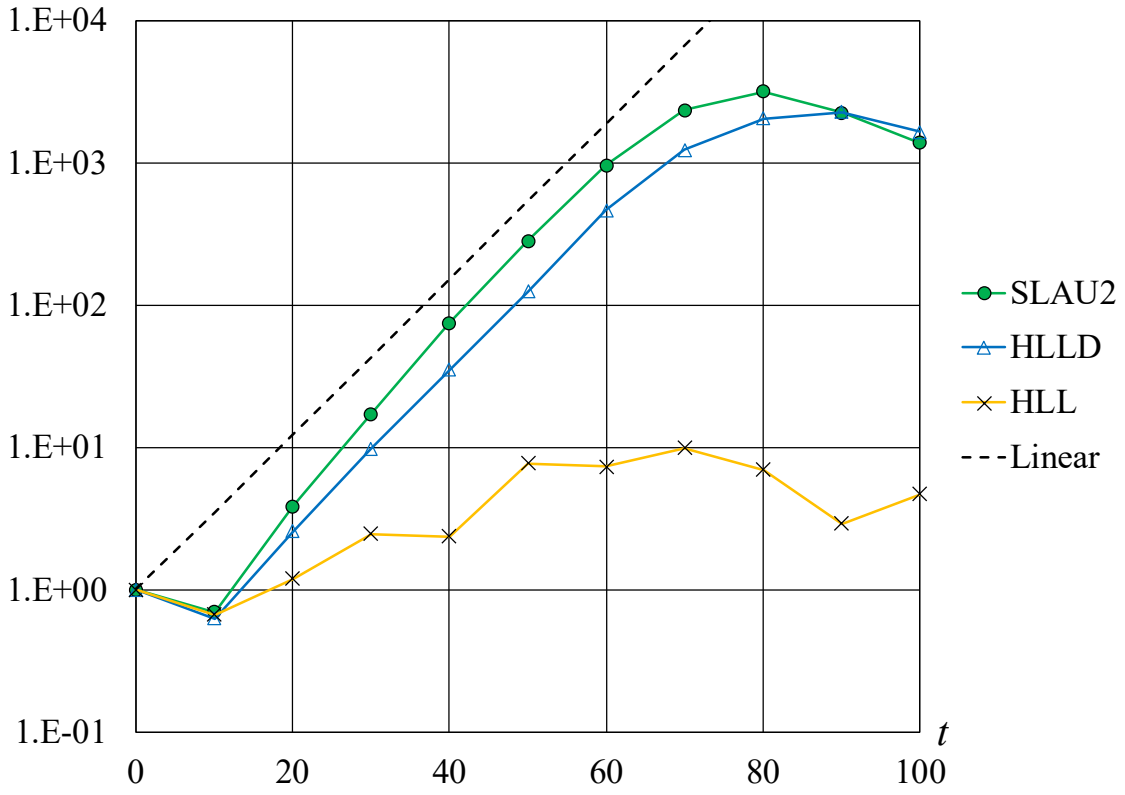

Fig. 18 Early Stage of Kelvin-Helmholtz Instability, growth rates of root-mean-squares of the *y*-velocity (normalized by each initial value).

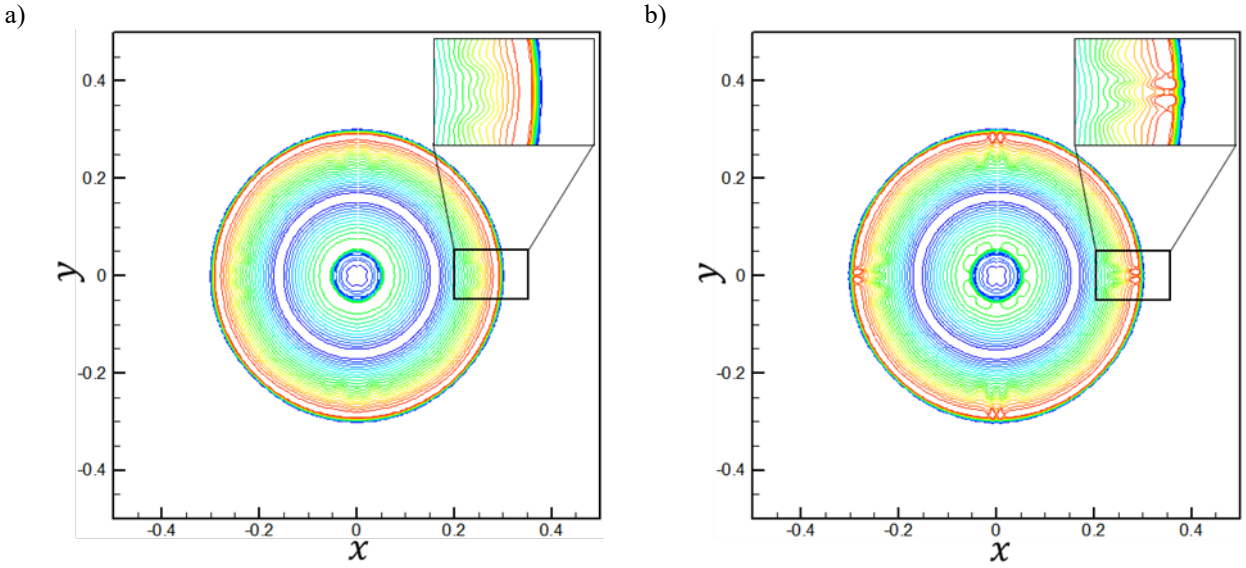

Fig. A1 HD Blast Wave Problem (t =0.01), velocity magnitude 0<|$\boldsymbol{u}$|<12.8, (a) SLAU2, (b) HLLD.

Table

Table 1. Computational Costs for Orzag-Tang Vortex Problem.

Numerical Flux	SLAU2	HLLD	HLL
CPU Time (non-dimensionalized by SLAU2 cost)	1	1.033	0.943